

April 2015

Radiolucent Loading Device for Computed Tomography Imaging

Andrew John Galanis
Worcester Polytechnic Institute

Joshua James Philippou
Worcester Polytechnic Institute

Nicholas Barreto
Worcester Polytechnic Institute

Follow this and additional works at: <https://digitalcommons.wpi.edu/mqp-all>

Repository Citation

Galanis, A. J., Philippou, J. J., & Barreto, N. (2015). *Radiolucent Loading Device for Computed Tomography Imaging*. Retrieved from <https://digitalcommons.wpi.edu/mqp-all/3091>

This Unrestricted is brought to you for free and open access by the Major Qualifying Projects at Digital WPI. It has been accepted for inclusion in Major Qualifying Projects (All Years) by an authorized administrator of Digital WPI. For more information, please contact digitalwpi@wpi.edu.



Project Number:

KT1-AAND

Radiolucent Loading Device for Computed Tomography Imaging

A Major Qualifying Project

Submitted to the Faculty

of the

WORCESTER POLYTECHNIC INSTITUTE

in partial fulfillment of the requirements

for the degree of

Biomedical Engineering

By

Nick Barreto,

Andrew Galanis,

Joshua Philippou

Advised by Professor K. Troy

Date: April 30, 2015

This report represents the work of WPI undergraduate students submitted to the faculty as evidence of completion of a degree requirement. WPI routinely publishes these reports on its website without editorial or peer review. For more information about the projects program at WPI, please see <http://www.wpi.edu/academics/ugradstudies/project-learning.html>

Abstract

There is a limited availability of portable compressional loading devices, none of which work within a computed tomography (CT) scanner. This is due to the lack of radiolucent materials these devices are made of, which make artifacts that disrupt the final CT image. Combining both testing and imaging can advance understanding of how materials behave at a microstructural level. This paper describes the design and fabrication of a novel device that can be used within a CT scanner to collect images of compressed bone samples. Validation testing showed that specimens could be compressed up to 2000 Newtons of force over 26 millimeters of displacement within 8 Newtons and 0.071 millimeters of accuracy.

Table of Contents

Abstract.....	i
Table of Contents.....	ii
List of Figures	iv
List of Tables	iv
Authorship:.....	v
Acknowledgments	vi
Chapter 1: Introduction.....	1
Chapter 2: Literature Review.....	4
Bone Imaging techniques:	4
CT Scanning:.....	11
FE Analysis:	13
Materials Testing Machines:	16
Stepper Motors:.....	17
Load Cells:	18
Displacement Sensors:.....	19
Chapter 3: Project Strategy	21
Initial Client statement:	21
Client Need and Wants:.....	21
Revised Client Statement:	21
Objectives:	22
Constraints:	25
Project Approach:.....	26
Chapter 4: Alternative Designs.....	28
Needs Analysis.....	28
Function Specifications.....	30
Feasibility Study	31
Conceptual Designs	31

Design Calculations.....	33
Decisions.....	34
Optimization	35
Preliminary Data.....	37
Chapter 5: Design Validation.....	40
Circuit Validation	40
Load Cell	41
Stepper Motor.....	45
Displacement Sensor	45
Chapter 6: Discussion.....	50
Assumptions.....	50
Precision and Accuracy	50
Limitations	51
Impact of Our Device.....	53
Chapter 7: Final Design and Validation	57
Chapter 8: Conclusions and Recommendations.....	61
Conclusions.....	61
Recommendations.....	61
References	64
Appendix.....	67
Engineering Drawings	67
Bill of Materials	72
Block Diagram	72
Stepper Motor Code	73

List of Figures

Figure 1: Young's Modulus in comparison to the calcium content of collagen fibrils [5].	5
Figure 2: Different classifications of distal radius fractures. [9]	7
Figure 3: Radial distal fracture pre and post-surgery. [13]	8
Figure 4: CT Imaging Basic Process. [18]	12
Figure 5: Hounsfield Scale. [20]	14
Figure 6: Compressive button load cell [29]	19
Figure 7: Image of an Eddy current proximity probe [30]	20
Figure 8: Image of an LVDT [30]	20
Figure 9: Design objectives tree	22
Figure 10: Initial design	33
Figure 11: Operational-Amplifier Circuit for Button Load Cell	41
Figure 12: Force to Voltage Comparative Chart	43
Figure 13: Expected curve if free moving plate does not deform.	44
Figure 14: Set up for LVDT validation testing.	47
Figure 15: Displacement to Voltage comparative graph.	47
Figure 16: Theoretically determined LVDT plot.	48
Figure 17: Block diagram of user interface	49
Figure 18: LabView Force and Displacement Graphs.	59
Figure 19: Top view of final prototype	60
Figure 20: Initial design	67
Figure 21: Final design assembly.	68
Figure 22: Motor plate cross section	69
Figure 23: End and free moving plate cross section.	70
Figure 24: Lead screw assembly	71
Figure 25: Block diagram of circuitry	72

List of Tables

Table 1: A comparison of different imaging techniques [16]	11
Table 2: Pairwise comparison chart of objectives the device needs to meet	25
Table 3: Actuators	35
Table 4: Load Cell Specifications	37
Table 5: LVDT specifications	38
Table 6: Linear actuator specifications	39
Table 7: Bill of Materials.	72

Authorship:

All members contributed equally on the entirety of this project.

Acknowledgments

We would like to formally thank our advisor, Professor Karen Troy, for her constant guidance throughout this project, our lab manager Lisa Wall for her help with gathering supplies and granting us access to facilities, the Race Depot for their help with machining our prototype, and Adriana Hera for her help with our LabView program.

Chapter 1: Introduction

Models developed by computed tomography (CT) imaging and computer modeling systems are commonly used in understanding mechanical and material properties of objects or elements in detail. CT imaging collects 2D x-rays in an arc around a physical structure and compiles the images into a 3D stack of grayscale slices. By assigning values to the greyscale that correspond to the bone density a new 3D map can be created which better represents the specimen. Programs like Mimics can be used to turn these 3D maps into a computer model for use in finite element (FE) analysis. FE analysis allows the user to simulate the effects of forces and moments on such models. Being able to simultaneously compress bone and image its microstructure could provide new insights into the way bones behave. By understanding the geometric properties of the structures, computer models can be created to mimic the structure. These models can be used to simulate complex forces that would be difficult to experimentally generate. These simulations can demonstrate how these structures are going to deform to help predict failure origins. By understanding bones on a microstructural level, innovations within the field of medical implants can be more easily achieved. With such testing, understanding of materials and mechanical properties of objects, in this case bone is available for use in projects. Validated models can help in the design of new medical implants, such as volar locking plates or distal radial implants, by identifying key points in the bone or medical implant structure that should remain intact or heavily supported. These key points are on the micro-scale and could not be analyzed with a lower resolution model. After recognizing these key points, implants that would damage or remove the supporting structures could be ignored in favor of other implants. Those discarded implants would have a higher chance to fail because they negatively affected the

bone structure. By improving medical implants based off of these findings, there is a lower chance of the implant failing or harming the physiology of the patient [1]. However, validation of computed FE models, either through literature or practice, is highly stressed to determine the rationality of the data produced [2] and [3]. The validation of FE models has been done through a variety of methods. The most common is to build a model of some object or materials that has been experimentally determined and comparing the FE results with the data. Bone structure has been examined using the CT scanner in previous cases; however, there has not been a direct point to point comparison of bone deformation in a FE model and an experimentally determined model. Without the direct point to point comparison there is a disconnection between the models being compared and how they were created. The direct comparison of FE modified models to an experimentally determined model generated with the same techniques as the FE model would help validate the software more definitively. This comparison could lead to more accurate simulations, if mistakes are found within the simulation.

The overall goal of the project is to design and build a device that can apply up to a two thousand Newton compressive force on a cadaver forearm specimen during CT imaging. This is beneficial for the purpose of eliminating discrepancies between current models and experimental models. Simultaneous testing and imaging will aid in optimizing the properties and design of materials intended for biomedical applications. The initial scan of an unloaded bone specimen will be obtained after placing the specimen in the device. A static compressive force will then be applied to the specimen, after which the specimen can be scanned. A potential use of this device will be validating current FE models of bone microstructures. A point to point analysis is done after scanning in order to compare the amount of displacement a bone endures from an experimental model to similar displacements found using FE software. One way this might be

done is to put both models on the same coordinate system and see how many points do not match between them. This will determine whether the model produced using FE analysis software is accurate and reliable. A device will be fabricated and used to create the experimental model necessary to validate the FE simulated model. The device must be able to apply the static compressive force directly to the specimen. It must sense the changes in force and displacement and communicate these changes to the user. Some of the factors limiting the device are size and material. The bore of the CT scanner being used is mostly closed off from the outside, so the device must fit and operate within the scanner. The device must be made of material that does not interfere with the imaging. The device should be able to load up to 2000 newtons of force, and measure the force applied and displacement within five newtons and 0.1 millimeters respectively. Accurate measurements are important because the FE simulation is ideally run under the same conditions as the specimen.

The Project is split into eight chapters. This first chapter is a brief overview of the project. The second chapter presents and explains relevant background information on the problem. Chapter three is a step by step explanation of how the problem was understood and how it was approached. The fourth chapter explains the various designs that were conceptualized to address the problem and the thought process behind why one design was developed over the others. Chapter five will display all of the collected data from experimentation to verify that the loading device works and meets the design specifications. The sixth chapter will be a discussion between the results and testing methods of previous work from literature to the methods and results gained from the loading device. Chapter seven discusses the final model we built and our reasoning behind our final design decisions. Concluding the report is chapter eight, providing a summation of the project and future recommendations.

Chapter 2: Literature Review

Bone Imaging techniques:

The human physiology consists of many different classifications of bone. Mineralized collagen fibril is considered the building block of bone, and constitutes the classifications based on the structure layout of these fibrils. Collagen fibrils are commonly found in other biological structures such as skin, tendons, and other soft tissues. The mineralization of collagen fibrils is due to a combination of carbonated apatite and water. The structural characteristics of the different types of bone are due to the layout of mineralized collagen fibrils, such as the density and porosity of the interconnected structure. In addition, proportional distribution of the water to mineral content of the collagen fibril has an effect on the mechanical properties of the structure. The results presented in [4] demonstrate a correlation between the increase in calcium content and a higher Young's modulus. The increasing concentration of crystals leads to a more fortified structure by decreasing the work under the stress-strain curve (Fig. 1).

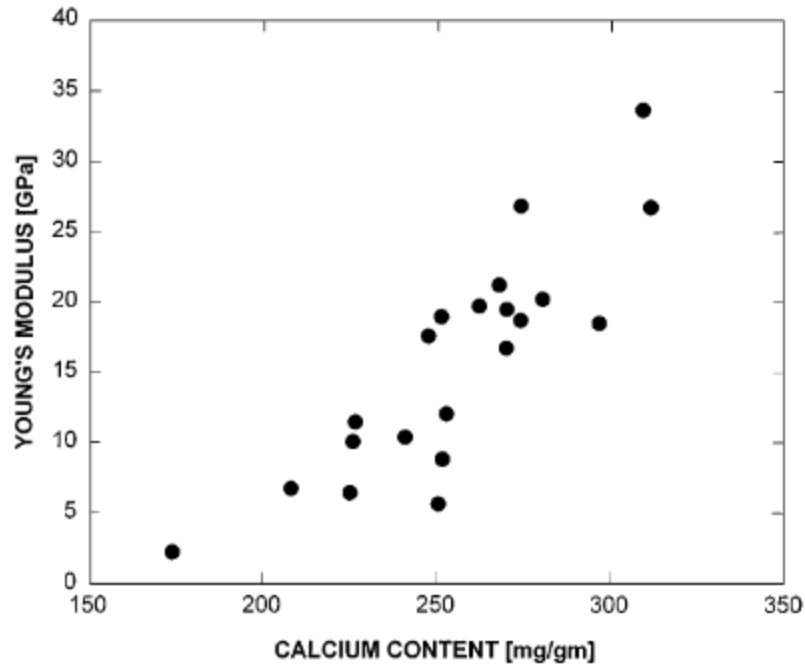


Figure 1: Young's Modulus in comparison to the calcium content of collagen fibrils [5].

The stacking of mineralized collagen fibrils creates a fibril array. The fibril array can be organized into several patterns depending upon the bone's function. Cylindrical motifs, also referred to as osteons, are hollowed out through the patterns and allow the blood vessels to reside in the bone. At a greater structural level, spongy and compact bone is differentiated based on the packing density of the fibril patterns.

Examining more specifically the radius, one can identify several classifications of bone including cortical and cancellous (trabecular). Cortical bone is highly condensed bone that forms the outward shell of a whole bone structure. Through means of ultrasonic and mechanical testing [6], cortical bone has been reported to attain an average Young's modulus of 20.7GPa (S.D. 1.9) and 18.6GPa (S.D. 3.5) respectively. The Young's modulus of cancellous bone was similarly calculated to be 14.8GPa (S.D. 1.4) and 10.4 (S.D. 3.5). Some researchers hypothesized previously that cortical bone is considered densely packed cancellous bone [7]. There is a significant variation between the reported findings, suggesting a non-correlation between the two

different classifications of bone. However, the publication also states that drying the bone samples before evaluation could have a possible effect on the mechanical properties of the trabecular structure. Regardless, there are other studies conclude a similar significant difference in the modulus measurements between cortical and cancellous bone [8]. This significance could be attributed to the difference in microstructure, mineralization, and the orientation and packing differences of the collagen fibers. The porosity difference between cortical and cancellous bone also provides a logical explanation for the differing mechanical properties and functions.

Factors such as the mechanical properties or the mineral density not only determine the functionality of the bone, but also how it deforms and eventually fractures. Based on the Muller AO Classification of Fractures, there are several different classifications for fractures in the distal radius. The main categorical fractures are extra-articular, partial articular fracture of radius, and complete articular fracture of the radius. The classification of the fracture is dependent upon certain fracture characteristics such as the displacement of the microstructure or the bone (Fig. 2).

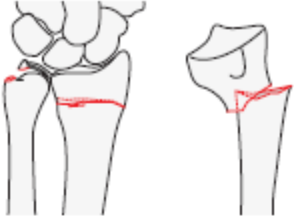
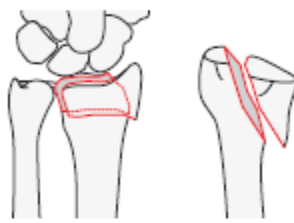
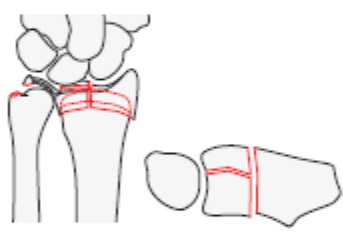
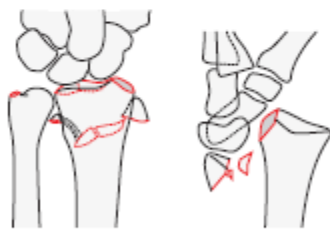
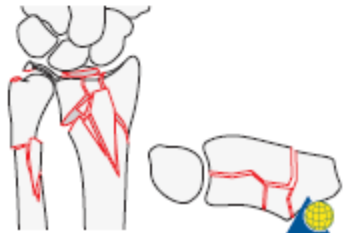
Type I Bending fracture of the metaphysis	
Type II Shearing fracture of the joint surface	
Type III Compression fracture of the joint surface	
Type IV Avulsion fractures, radiocarpal fracture, dislocation	
Type V Combined fractures (I, II, III, IV); high-velocity injury	

Figure 2: Different classifications of distal radius fractures. [9]

While the fracture consists of a failure in the microstructure of the trabecular bone, the initial formation of a macro crack in the cortical bone defines the starting stages of a fracture [10]. In order for the fracture to heal, the body must undergo a clotting process around the affected area. Depending upon the severity of the fracture, the body has the possibility of healing

itself but with differing results. Studies show that the displacement of the bone microstructure can change the functionality of the wrist region [11]. In addition, the differing treatments of distal radius fractures are reported to change the outcome of functionality in the wrist [12].

There is a wide variety of noninvasive and surgical methods of treating distal radius fractures. Medical implants have been commonly used for the repair of distal radius fractures in more severe cases (Fig. 3).



Figure 3: Radial distal fracture pre and post-surgery. [13]

Medical devices for distal radial injuries can be fixated both externally and internally; the method of treatment is determined by the classification of the fracture. When utilizing internally fixated implants, there should be a consideration for different design features and their associated benefits and constraints. For example, screws or pins can be used for the fixation of the locking-plate implants for distal radial fractures. Mechanical testing and patient studies have been conducted to understand differences in surgical techniques and design features of locking-plate systems for distal radius injuries [14] and [15]. For example, a comparison of failure loads in

principle motions was conducted between locking smooth peg and locking screw configurations for fixation of a distal radial implant [14]. However, there is limited research that considers how the fixation of these implants may change the trabecular structure. Understanding the interface between the implant and the fractured bone could lead to implications that certain devices may cause more damage, and implant failure in more serious cases.

Video Microscopy uses simple optics and video to create images of the bone microstructure. Light is projected through a bone segment and captured to a video. This method can be useful for seeing bone macrostructure and some of the microstructure, but the low penetration makes it difficult to image large sections of the bone. The only way to create a 3D model with this technology is by using histological sections of the bone and compiling the 2D images into a larger model. This destroys the bone in the process which makes further testing impossible. The sections would be so thin that loading the section slightly would create large stresses. It would also be difficult to load the samples and not disrupt the apparatus' imaging.

X-ray radiation based imaging technologies can overcome the low penetration the protons face. Without the use of computers to compile the images radiography can only produce 2D images. The x-rays penetrate soft tissue easily but are partially blocked by the denser bone material. This partially blocked x-rays appear as whiter areas on the image. By using a grey scale a level of density can be determined for those bones. By taking multiple x-rays from different angles the various 3D structures can be created by compiling the many different 2D images. To increase resolution an increase in radiation and computational power is required. The increased radiation will penetrate the bone and make distinguishing the microstructure within the grey scale easier. This increased resolution creates a lot more data that the computer has to use to create a 3D model. While the technology does not require the bone to be destroyed prior to

imaging it does generate radiation that can damage the bone and change its properties. The slight amount of radiation that the bone is exposed to for the testing done by this project should be kept in mind during data analysis, but it should not dramatically change the results. The last main limitation of CT imaging is that the material surrounding the bone cannot be too dense or it will block the x-rays and distort the image.

Scanning electron microscopy uses a focused electron beam to penetrate and image specimen. It is capable of viewing images in much higher resolution than any of the other imaging technology. The electrons interact with the atoms of the specimen and produce various signals that can be captured and processed into high resolution images. It suffers from the same drawbacks as light microscopy when it comes to bone structure because the electrons cannot penetrate the hard calcified bone. To accurately image the bone microstructure the bone must be cut into thin slices. This makes loading the bone as a whole impossible.

Atomic force microscopy uses a tiny lever that is flat on top and comes to a point on the bottom to map the surface of a specimen. An electron beam is focused on the flat part of the lever head and deflects to a sensor. As the lever moves across the specimen it may rise or fall and change the angle of deflection of the ion beam. This change in deflection angle is sensed and a nanoscopic change in elevation can be recorded. This method of imaging is good for producing a very high resolution 2D image of the bone. To image the bone microstructure a very thin slice must be cut from the bone. External forces cannot be applied to the specimen during imaging which is necessary for imaging loaded bone microstructures.

Table 1: A comparison of different imaging techniques [16]

Technology	Resolution	2D/3D	Destructive	Loading	Computer Model
Video Microscopy	20 nm	2D	yes	No	Yes
Radiography	5 micrometers	2D	No	Yes	No
CT Scanning	Millimeter to 1 micrometer	3D	No	Yes	Yes
Atomic Force Microscopy	50 nm	2D	Yes	No	No
Scanning Electron Microscopy	Up to 1 nm	2D	Yes	No	Yes

CT Scanning:

Computed Tomography is the use of a computer to generate a 3 dimensional model of a bone or other organ tissue using 2 dimensional sliced stacked on top of each other. The specimen is placed in the scanner which projects a fan of x-rays. The fan beam of x-rays moves around a 180 degree arc over the imaged length of the specimen. These x-rays penetrate the specimen and are collected on rotating detectors. The detectors then send a signal which a computer can read and a greyscale image is generated. As the scanner moves the x-ray source around an arc multiple 2D images of the specimen are captured at different angles. These different angles are compiled into a single 3D slice. The specimen is moved through the scanner so that multiple slices can be created allow the specimen. These slices are stacked on top of each other and compiled to create the final 3D model of the specimen. The grey scale is created based on the amount of radiation that reaches the detectors. As the x-rays pass through a specimen they can be blocked or deflected off of dense materials, such as bone. This lowering of radiation reaching that point of the detector signals that the image of that area should be whiter. This principle

allows for CT technology to map different densities in comparison to its surroundings. It is especially important for imaging the trabecular microstructure which has pores that appear as black areas or voids within the material [17].

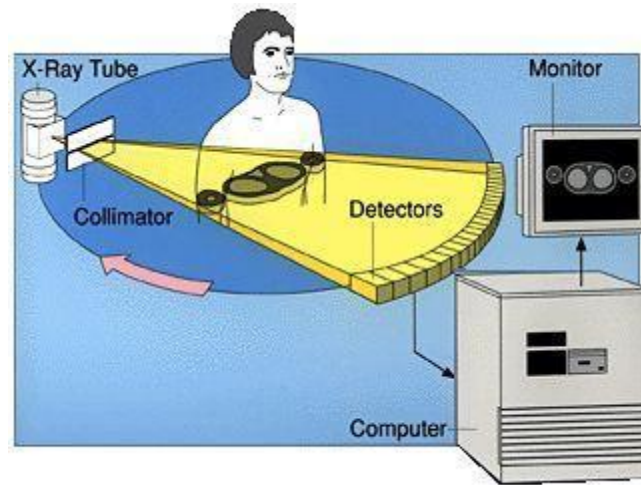


Figure 4: CT Imaging Basic Process. [18]

Osteoporosis is one of the diseases that CT imaging can help diagnose and classify. It is caused by bone demineralization which causes bone to lose density and mass. By taking CT scans over a period of time the changes in bone density can be tracked and analyzed to determine possible risks different individuals face. One study looked at the long term affects astronauts face in an extended stay in zero gravity. By suspending rats by their tails the authors simulated a loss of mechanical loading in the rat's legs. They then imaged the rat's tibia bone using micro-computed tomography over three weeks. It was clearly visible that the rat's bone was losing density as the trabecular portion of the bone got darker and disappeared over time. It was also shown that a decrease in bone density had a direct impact of the bone's mechanical properties. This impact included a 15% decrease in bone volume, a 25-40% loss of trabecular bone mineral density, and a loss in structure. These factors weaken the bone and make it more susceptible to breaking. It is important to image bone microstructures because the bones mechanical properties

can be estimated using its density. Its density can be mapped using the gray scaled image produced by the CT scanner [19].

FE Analysis:

The computer generated model can then be imported into other programs for further analysis and use. The generated models can be used to see what happens in a theoretical case that would be difficult to create experimentally. It can combine different loads on the models and show how the models will deform and what areas will carry the most stress.

A program developed by Materialise known as Mimics has been widely used for recreating 3D models from CT scanned images. DICOM format is primarily used for the development of the scans, and usually include patient data as well unless previously de-identified. DICOM images are different from other image formats (.jpeg for example) as they can be used in 3D modeling programs. The cross-sectional images are stacked and implemented into the Mimics program, and are displayed in several viewpoints: coronal, axial, sagittal, and 3D. The axial view is the original stack of DICOM images. The coronal and sagittal views are generated by the Mimics program based off of the original stacked images in the axial view. The 3D greyscale image is produced based off of where the user decides to establish an origin point on the images. The property differences in the greyscale images are rendered using the Hounsfield Scale, which includes 4096 values that define certain materials (Fig. 5).

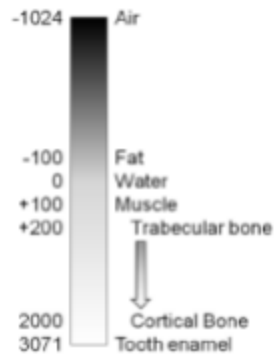


Figure 5: Hounsfield Scale. [20]

The Hounsfield scale applies material properties based on the shading of the greyscale model per pixel and is directly proportional to the density of the imaged material. By using this scale, the user can create a 3D model using several segmentation techniques for separating certain materials from one another. Thresholding is a process of separating the greyscale image material properties using predetermined values. Thresholding allows the user to color code the images based off of the Hounsfield Scale, which defines pixel properties based on the shading of the material. Color coding aims to help separate the model based on the assigned pixel value. There are many tools that also separate the pixels of the DICOM images such as Dynamic Region Growing, in which the program color codes the image for the user based off of the assigned pixel properties of the greyscale model. If the thresholding does not satisfy the user, then the user can easily edit the coloring or ‘masking’ of the image. The greyscale image can also be limited to a certain range within the Hounsfield Scale to eliminate voxels that do not contain appropriate greyscale values would not be used in the final model.

The Mimics can export the meshed models to a finite element analysis (FEA) program. Utilizing the Hounsfield Scale the user can assign material properties, as this method correlates the color scale in DICOM images to the density of materials such as bone.

In order to accurately predict the deformation of the model before a finite element analysis is conducted, kinematic constraints must be applied to the model. In other words, the model is suspended in free-space until the model is fixated by a plane, axis, or specific points on the model. Once the model has been fixed, loads and moments can be applied to different places on the model. Forces or moments can be applied to single node points on the model, or to a group of node points. Several types of loading or analysis of the model can be applied including the following: linear statics, nonlinear statics and dynamics, vibrations, dynamic response, buckling, and heat transfer. Once the FEA has been conducted, the model will be discolored and deformed, demonstrating the effect of the applied loads on the model. The discoloring is measured by a scale that demonstrates the magnitude of elemental forces, strains, stresses, nodal displacements, velocities, or accelerations applied to the model [20] and [21].

FEA models allow for the possibility to understand the nature of materials when the outside environment is interacting with them. Bones are consistently used in finite element models to better understand the deformation of bone under certain applied loads. There are benefits for using FEA and the knowledge of bone deformation to help guide clinical research or innovation. For one, implants modeled in FEA with bone can be used to understating the interactions between the implant and the microstructure. This can aide in the prototype stage of medical implants by testing their mechanical capabilities and interaction with bone before it arrives to the market. Thus, the development of devices that would fail in clinical trials would be more limited, and save money for research and development in medical corporations. FEA also allows the user to change the environment of the model. When analyzing bone, many other physiological factors are associated near or in the model that can be used for further knowledge.

By changing the physiology, the user can understand how geometric additions, such as blood vessels, proteins, signals, and drugs, may affect the trabecular bone structure.

Validation studies for FE analysis generally start by developing a 3D model based on a real world experiment. The model is then placed under the same loading that the experimental model was, and the results are compared [22][23][24][25]. One such study that looked at trabecular bone failure and validation of FE models used this method. The fracture behavior was studied in comparison to a FE model. To do this, researchers created a 3D model in FE using a CT scan of their test subjects. They then applied a compressive force to the FE model to estimate the failure sites in the structures. After they generated a map of the expected failures they performed an experiment version of the simulation. They compared the expected ultimate stress and yield stress to 23 experimentally determined values, and observed a near 1 to 1 relationship. The researchers concluded that they could map the failure zones in trabecular bone using FE analysis and it would correspond to data found in the test. Some of the major limitations of this and similar studies are how they validated their FE models. This includes simplifying the experiment, ignoring tissue properties, and neglecting the viscoelastic behavior of bone. They simplified the FE model by making it isotropic instead of anisotropic. They ignored important tissue properties like mineral density and the geometry of the trabecular bone [22]. They use only 2D means of measuring strain to validate 3D models [22][23][24].

Materials Testing Machines:

Materials testing machines come in a variety of types depending on the material properties they are investigating. Testing devices have several similarities that are common among them. There is an area for materials or specimen to be placed and some form of gripping to hold it within the machine. Sensors are implemented to read and display applied forces, and

displacements. Finally some form of actuation to apply the loading and conduct testing is needed. There is a range within compression testing devices based mostly on complexity and cost.

The more expensive loading devices can perform multi-axial loading on a specimen to understand the effects of compression, tension and rotation. They have precise and accurate sensors to monitor the loads being applied and the motion of the loading. The grips that hold materials in place are interchangeable to allow for specialized grips based on the material and test. A computer controlled motor is used to actuate the device and apply loads. This allows the test to be controlled by an automated system. Depending on the company different user interfaces control the devices, as well as display and record data from testing.

Cheaper testing devices have much less usability or features. They mainly consist of only the of a compression sensor and on displacement sensor. The actuators are manual hand cranks, and the grips are simple plates for the material to rest on. The displays do not all record and store the data, but simply display it to the user.

To better understand commercial loading devices, their individual components were researched in more depth. The first component was a linear actuator to apply the force, specifically motors. Next, load cells and displacement sensors were researched to understand how they work.

Stepper Motors:

Linear stepper motors allow the linear movement of a threaded shaft or lead-screw utilizing internal rotary components. As the rotor rotates, it moves the threaded shaft in a linear motion. This linear movement thus produces a linear force to objects if fixated to a surface. The amount of force applied linearly depends upon three factors in the threaded shaft: the lead, pitch,

and diameter. The lead of a threaded shaft is the axial distance required for the shaft to make a single rotation. The pitch is the distance between thread levels. An increase in lead distance allows the stepper motor to generate less driving force due to the decreased amount of threads per inch [26]. The required power to generate a certain driving force is shown in the equation below:

$$P_{\text{linear}} = \frac{(\text{distance traveled in meters}) (\text{force in Newtons})}{(\text{Time to travel the distance in Seconds})} = \text{watts} \quad (1)$$

Linear stepper motors can be powered by different means including hydraulic, electric, and through electromagnetism [27]. Each power option for the stepper motor has its benefits and shortcomings depending upon the application that the motor will be used for. Electromechanical test machines, such as those developed by Instron, are similar to linear actuators in which case an applied force can be generated upon an object using electrical signals sent by a linear actuator driver [28].

Load Cells:

Load cells are transducers that generate a signal that is converted from electrical energy into a unit of force. Common load cells used for measuring compressive forces are button load cells that include a strain gauge. Strain gauge load cells work by applying loads to a Wheatstone bridge configuration within the sensor. The applied load causes the strain gauge to deform, creating a change in voltage that can be measured. This voltage output can be scaled and converted to show the approximate amount of force being applied to the load cell in units of force. [29]



Figure 6: Compressive button load cell [29]

Displacement Sensors:

Displacement sensors are another form of transducer that converts electrical signals into units of length. These devices are capable of collecting high resolution measurements of the position or change in position of a given object. Common types of displacement sensors include Eddy current proximity probes, linear variable differential transformers (LVDTs), and rotary variable differential transformers (RVDTs).

Eddy current proximity probes measure the relative proximity of an object. From a mounted position on a mechanical structure, proximity probes utilize voltage changes to measure rotating or reciprocating shaft surfaces. The probe works by emitting a constant electromagnetic field. As the probe gets closer to a conductive object a distortion in the field can be measured by the probe. Depending on the size of the distortion, displacement can be interpreted.

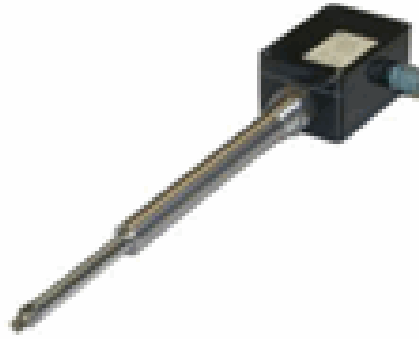


Figure 7: Image of an Eddy current proximity probe [30]

LVDTs utilize a stationary coil assembly and a central core that is free to move. Signal values are generated based on the position of the central core in the LVDT tube. A sine wave is formed for the primary output signal while a secondary output signal is demodulated. After passing the demodulated signal through a lowpass filter, a DC voltage is outputted that is proportional to the central core's displacement. RVDTs are the rotational derivative of an LVDT and are usually operable in a 30 to 70 degree angular range. [30]



Figure 8: Image of an LVDT [30]

Chapter 3: Project Strategy

Initial Client statement:

Design and fabricate a device that can apply compressive forces of up to two kilo Newtons to cadaver forearm/hand specimens. The device must include sensors for measuring force within five newtons and displacement within 0.1 millimeters. It must fit inside the bore of the CT machine, and all portions of the device that surround the specimen must be radiolucent, meaning they should not be made of metal or other very dense materials.

Client Need and Wants:

The client needs a device that can apply a compressive load to a forearm specimen while imaging it in a CT scanner. The device must not block the imaging of the bones microstructure. The client wants to use the device to image the microstructure of a loaded distal radius and analyze the images. The goal of the project is to design and fabricate this device and verify that it functions properly. To do this, the device must be able to accurately sense and record the force being applied to the specimen and the displacement of the system.

Revised Client Statement:

Design and fabricate a device that can apply static compressive forces of up to two kilo Newtons to cadaver forearm/hand specimens while it is being imaged by a CT scanner. The device must not interfere with the imaging process and be able to measure and record the force within five Newtons and displacement within 0.1 millimeters.

It is necessary to break down the primary goal of fabricating a radiolucent compressive loading device into objectives and constraints. This is not only useful towards understanding what secondary goals the device should achieve in the efforts of completing the primary objective, but also the limitations that will affect the overall final design. The main goal has been broken down into six main objectives, as seen in Fig. 9 below.

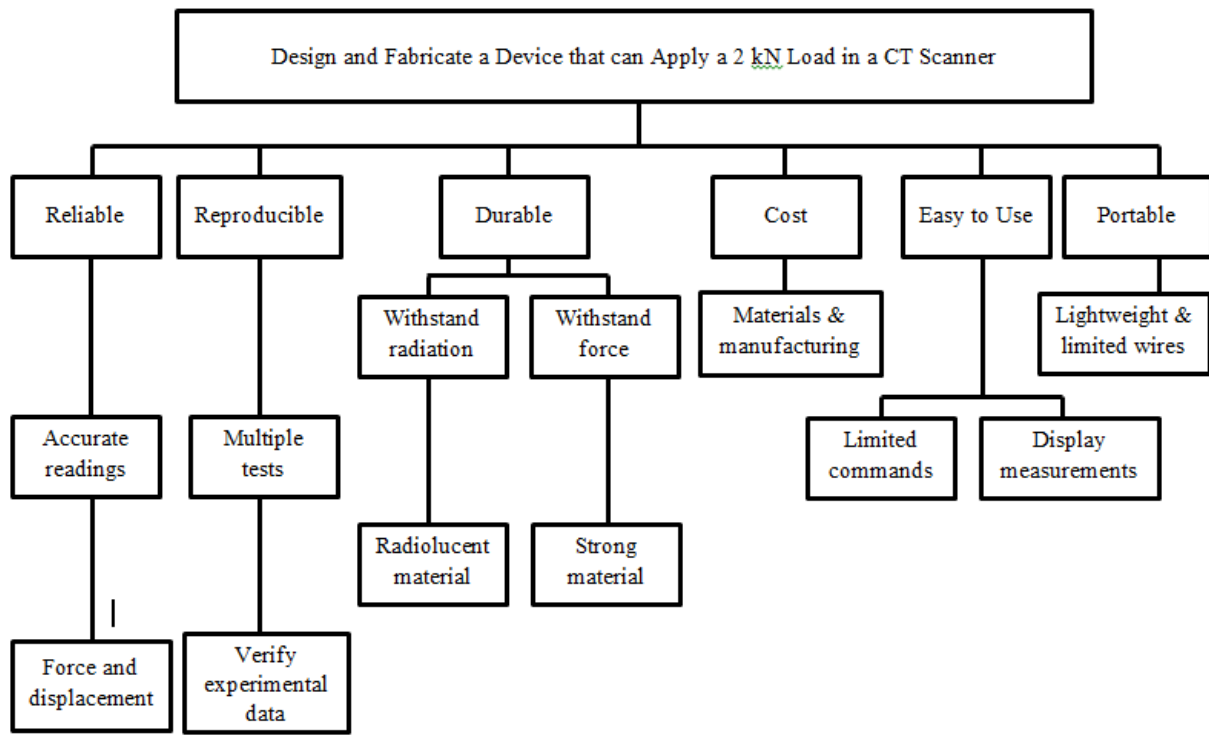


Figure 9: Design objectives tree

Objectives:

Reliable: In order for the device to be reliable, it must provide the user with several secondary-objectives: an accurate *force reading* (within five Newtons of force), and an accurate reading of displacement (within 0.1 millimeters). It is important for the device to be reliable so that the data produced is an accurate representation of the specimen and it is useful for the study at hand. Data that accurately represents the loaded specimen is necessary in order to compare with and validate data from current FE models.

Reproducible: The device needs to be able to perform multiple tests on a single specimen and produce similar deformation results each time. It is also important for the device to be able to test various specimens to show similar results between them. If the deformations between each specimen are not similar, it will provide haphazard data that

will not be able to produce an accurate image of the deformed microstructure. The results obtained from multiple tests should be similar in order to confirm that the data serves as an accurate model for the loaded specimen. The experimental data can then be used as reliable evidence that verifies current FE models.

Durable: The materials used for the device must withstand the radiation of the CT scanner for multiple uses, of up to 100+ tests. Therefore, it is imperative that radiolucent material is used to build the portions surrounding the specimen. A proper CT image and accurate data cannot be obtained if the bone sample is hidden from view by a very dense material such as metal. In addition, the device needs to be durable, as the amount of force applied to the specimen will require strong materials so that the device will remain intact from the applied load of up to two kilo newtons. If the device does happen to break, then it must be easily repairable with common materials to prevent major postponement of research.

Cost: All costs related to the project cannot exceed \$1000. Manufacturing and prototyping costs have to be taken into consideration, as well as which bone samples are used for testing. It is important to keep manufacturing costs low so that many units of the device can be made for sale. It is also important to keep costs under \$1000 or the project will not be completed.

Ease-of-use: The device has to be simple enough for an average client to use properly on the first try. To make the device more user friendly, it will utilize a limited set of commands. Also, the device will include a feature that communicates with the user that displays force and displacement measurements. Ease-of-use is important so that clients will not be frustrated while using the device, especially if it is going to be used regularly.

A simple device can ensure that multiple tests can be performed often so that many samples of experimental data can be obtained. Comparing the large amount of data can verify whether or not the data being produced is accurate and suitable for comparison with current FE models.

Portable: The device will be taken out of the CT scanner constantly so it must be easily transportable. In order to provide a portable device, the prototype must be light weight so that the user will not have an issue taking it out or putting it in when specimens need to be changed. In addition, the device must be small to fit inside the bore of the CT scanner. Since the device will be a controlled gadget, there will be an outside entity or connection to a control or computer. The device must either have limited to no wires that connect it to a processor so that the user will not be frustrated with a considerable amount of tangled wiring to fumble with.

After ranking the objectives with a pairwise comparison chart, Figure below, reproducibility and reliability were determined to be of the highest importance followed closely by durability. Cost, ease of use, and portability were of lesser concern because they did not directly impact the results of testing. Reproducibility and reliability are the same in terms of importance. Durability followed behind since it is highly important that the device does not break or malfunction during or after testing. Reducing the cost, while being an important consideration, was not ranked highly since it is not a big factor on how the device will perform.

Table 2: Pairwise comparison chart of objectives the device needs to meet

	Reproducibility	Reliability	Durability	Cost	Ease-of-Use	Portability	Total
Reproducibility	X	0.5	1	1	1	1	4.5
Reliability	0.5	X	1	1	1	1	4.5
Durability	0	0	X	1	1	1	3
Cost	0	0	0	X	1	1	2
Ease-of-Use	0	0	0	0	X	1	1
Portability	0	0	0	0	0	X	0

Constraints:

Under \$1000: The budget for the entire project is 1000 dollars. All the prototyping, materials, and testing specimen must not cost more than 500 dollars. The extra 500 dollars is for unforeseen problems with the prototype and its redesigns.

Dimensions: 31” by 5” by 7.5”. The device and specimen must fit within a 31 inch by 5 inch by 7.5 inch box. This is the maximum dimensions of the CT bore and exceeding them will prevent the device from being placed into the scanner.

Materials: The materials surrounding the specimen must be radioluminescent so that it will not interfere with the x-rays. Material that is too dense for the x-rays to pass through it will block the imaging of the bone and its microstructure. This limitation is only around the 9-11 centimeter slice of the specimen being imaged so the rest of the device can be made of non-radioluminescent material.

Loading Capacity: The load sensor must be able to sense forces of up to two kilo Newtons without being overloaded. This limits the sensors that can be used to measure the force generated by the device.

Loadbearing on materials: A lot of the material within the device will be under a tensile load of up to two kilo Newtons of force. Materials that cannot support that load without deforming are not suitable for the device.

Project Approach:

The success of the project is dependent on the organization and details of the approach throughout the year. For this project, a timeline was set for what was to be accomplished each term. A-term consisted of three primary goals: revising the client statement, researching background material, and completing design drawings.

One of the objectives in A-term was to breakdown the initial client statement. This was done in order to get a better understanding of what the client wants to be produced by the end of the project timeframe. Speaking with the client helped determine unmentioned specific details that had to be taken into consideration during the initial design stages. Questions raised during client meetings also helped to advance the other major goal for A-term, background research.

It was very important to complete all of the background research on information relevant to the device and as to why it is needed in the first place. Research was done on various topics such as FE analysis, loading devices, CT scanners, suitable building materials, and clinical significance. By gaining a better understanding of these topics, it allows to see how they all relate in the context of the loading device project. Furthermore, objectives, constraints, and functions were determined during this stage of project. These are important factors that need to be considered when creating the initial hand and CAD drawings, since they can limit which design concepts to actually consider for prototyping in B-term.

The primary design for the CT loading device consists of two plates contained within a box made of radiolucent material. The radiolucent case will need to fit within the dimensions of

the CT bore, which are 7.5" x 31" x 5". One plate remains fixed at one end, while the other is able to move and apply a compressive force after it has received enough power. An electric motor was chosen as a power source because of better efficiency and lower cost in comparison to other power sources. Completing the prototype early will allow for more time to test. Undergoing enough trials will help in spotting any problems with the device. The device will be redesigned as needed in order to address any challenges.

Chapter 4: Alternative Designs

Needs Analysis

There are certain properties that the device needs to possess in order to meet the overall project goals. One of the top priorities is to ensure that the materials surrounding the bone specimen are radiolucent. This means that the material that surrounds the bone specimen cannot be very dense. This ensures that the specimen can be seen during the scan without the material absorbing or diffracting the x-rays. Materials of the device must remain mostly unaffected by the x-rays in the CT scanner so the device can retain durability after multiple uses. Taking this into consideration, this eliminates metal as a potential material that could be used to surround the bone specimen. Because of the large tensile stresses expected in the supporting structure that surrounds the specimen, ceramics can also be eliminated. This leaves plastics as the most viable option for the support structure.

Another important property to keep in mind is the size of the device. To scan and collect data, the device needs to be able to fit within the bore of the CT scanner and house the specimen. The dimensions of the CT bore are 7.5" x 31" x 5". The device will have to fit comfortably within the dimensions so the bone sample inside can be scanned.

There are specific loading requirements for the device. The device needs to be able to apply a compressive force of up to two thousand Newtons on the bone sample. The significance of the two thousand Newton force is that it is a magnitude where some failure in bone is observed. This maximum force was specified by our client as a suitable max for their application. When the device measures the force, it is also necessary that the magnitude is displayed to the user.

Lastly, the device has to be able to perform multiple tests. Successfully completing multiple tests shows that the device is reliable and can reproduce data. Collecting enough data after multiple runs will be necessary to validate the final prototype.

There are two different precision properties for the loading device that are desired for the purpose of displaying accurate results. The first is that the compressive force magnitude should be measured within five newtons. The second wanted property is for the displacement sensor. In terms of measuring displacement, the sensor should measure within 0.1 millimeters. This is beneficial in order to provide a precise measurement that is more accurate and reliable than one taken using a larger unit of length. Given the project's constraints, these parameters may not be completely feasible.

A list of constraints was determined in order to narrow down potential design ideas. For the project, the budget was limited to one thousand dollars. This will be able to demonstrate how the device can perform the desired functions using the most inexpensive parts. Keeping costs down throughout the project timeframe will be especially useful towards the testing stage. If the prototype fails, there should be enough funds to fix the situation through a redesign of the prototype. Low manufacturing costs will be an advantage if the device goes beyond the project and makes it into the medical industry. A low cost can guarantee that multiple units can be made for sale and that the distributor can make a profit.

Some of the parts that the device is composed of will need to be radiolucent. The main component that needs to be radiolucent is the one containing the bone sample. If the material surrounding the bone is made of very dense material, the x-rays in the CT scanner will not be able to reach the specimen. This is because the sample would be obscured from view and a proper image of the microstructure would not be obtained.

To obtain data, the device needs to be able to function inside the CT scanner. Therefore, it has to be able to fit within the CT bore where samples are placed. After obtaining measurements of the bore, it was determined that the device needs to fit within the dimensions of 7.5" x 31" x 5". It is important to make sure the dimensions for the loading device are close to the actual dimensions of the bore. This will help in stabilizing the device so that it does not move during scanning, eliminating motion artifact when images are taken. Also, using dimensions close to those of the bore allows users to place normally sized specimens in the bore as opposed to ones that do not resemble bones used in actual loading applications. This will give users results that can be applied to different patients as opposed to using models that would need to be proportioned properly for the purpose of comparing with actual human models.

Function Specifications

The device will be able to perform several key functions. The primary function of the device is applying a compressive force on a bone sample with a magnitude of up to two thousand newtons. To perform this function, the sample will be placed between two end plates. One will be fixed while the other is free to move within a one dimensional plane. The free moving plate will compress the bone until the desired displacement to be scanned is reached. When the device applies a static, compressive force, custom contours on the end plates will hold the sample in place to eliminate motion artifact while a CT scan is being performed.

Force displacement measurements will be taken and displayed to the user. A load cell will be placed between the two sheets that make up the free moving plate. When a force is applied to the bone sample, the load cell within the plates will be able to measure the magnitude and then display the reading to the user. A sensor will be used to measure the displacement after

the bone sample is compressed. Once the measurements are obtained and the scan is taken, an image will be created showing the microstructure of the bone under a compressed load.

Feasibility Study

Feasibility studies need to be performed in order to show that the various instruments on the device are able to produce actual, accepted values, and to demonstrate how well the instruments can repeatedly reproduce those values. To test the loading capabilities of the device, objects of known weight will be used to determine the force applied. Knowing this force, the same object will be used on the load cell that will be placed within the plates that hold the specimen. It can be assured that the load cell is functioning as intended if it returns the same magnitude value as the one obtained from utilizing the force plate. This test will be repeated several times to ensure accuracy and repeatability. The displacement sensor will also undergo feasibility testing to show that correct measurements are being taken up to the desired precision of 0.1 millimeters. A simple way to do so is to use a caliper while compressing a sample to a known length. A sample can be compressed again to the given length, but the measurement will be taken with the displacement sensor. If the sensor returns the known value of displacement, it will demonstrate that the position sensor is functioning properly and taking correct measurements.

Conceptual Designs

The final design was the end result of a seven week process involving discussion amongst the client and the design team. An initial design for the prototype was created after reading the client statement given at the beginning of the project and collective thinking amongst the group. After speaking with the client again to determine specific objectives, constraints, and functions

for the device, the client statement was revised. This revision helped in narrowing down choices to design ideas that were suited to meet project objectives, work within the constraints, and perform the desired functions. After redesigning the initial schematic for the device, a model was created using CAD, advancing the project to the preliminary design stage. Further discussion amongst the group aided in determining other aspects of the device, such as instruments used for measurements and suitable materials for fabrication. Once limitations were considered and it was determined that the device could achieve the goals of the project, the device advanced to the final design stage. The changes in the design can be viewed in the schematics below.

Max Sustainable Load for One Pipe

$$D_O = 27.22 \text{ mm}$$

$$D_I = 18.06 \text{ mm}$$

$$\text{Yield Strength} = 4.69 \text{ MPa}$$

$$4.69 \text{ MPa} = \frac{x}{\pi([\frac{1}{2}(0.02722 \text{ m})]^2 - [\frac{1}{2}(0.01806 \text{ m})]^2)} \quad (2)$$

$$X = 1527.14 \text{ N}$$

Decisions

The first aspect of the device that was designed was the method for compressing the bone sample. Initially, the design involved two endplates that the bone sample would be placed between. One endplate would be fixed while the other would have the capability of moving back and forth in one dimension. Instead of relying on the moving plate to stay in parallel with the fixed endplate, a redesign was done to include four rods that would connect the two plates at the corners. This way, the plates are on a rail system that keeps the moving plate from wobbling out of place. Not only does this add support for the plates, but it will also ensure that the bone sample does not fall out from between the two plates during loading and imaging.

To operate the device and enable the free plate to move, a proper actuator was required. Several types of motors were considered, including electric, pneumatic, and hydraulic. Due to certain limitations such as high costs and maintenance requirements, the list of potential power sources was minimalized. As seen in the table below, two motors in particular were examined for possible use as well as a manual hand crank in the fabrication of the radiolucent loading device: linear stepping and hydraulic. It was decided that a linear stepping motor would be the best

possible solution to applying a static force. This is based on an evaluation of the different motors, which examined design specifications such as the required power source and purchase price.

Table 3: Actuators

Actuator	Power Type	Force (N)	Price (\$)
Haydon Kerk Linear Stepper Motor Size 34	Electric Motor	2000+	252.52
Hydraulic Cylinder	Hydraulic Motor	4000+	390.00
Hand Crank	Manual	User Dependent	~50

Due to the limited budget, it was decided that the linear stepper motor would provide the best solution for this application. The hydraulic cylinder was considered due to its larger applied compressive force; however, the objective of the loading device is to compress bone samples up to 2kN. In addition, the hydraulic cylinder would require its own source of power based on a pressure gradient to retract and extend the piston. The required amount of pressure applied in the hydraulic cylinder to reach larger compressive forces also poses a problem, as certain hydraulic power sources output differing magnitudes of pressure. A hand crank was also considered since it is a cheaper and reliable form of actuation. An electric linear stepper motor was chosen because it was the cheapest automated actuator available. The use of a prototype motor to understand the programming of the electric motor was also considered. However, it was decided that the cheaper alternatives for linear stepper motors would not provide sufficient data to equate to larger motors that would have different required input voltages to operate.

Optimization

A set of specifications was determined in order to create the best product possible for the chosen design configuration. After measuring the size of the CT bore, the proper dimensions for

the loading device were acquired (7.5" x 31" x 5"). Materials chosen for the device were picked based on cost, reliability, and radiolucency. The material for the endplates was steel. Steel was chosen since it is a material that possesses strong mechanical properties that allow it to apply the large compressive force that is required. While metals such as steel are not radiolucent, this was not seen as a major issue since the plates are holding the sample in space. The x-rays within the CT scanner will have plenty to image since the metal endplates are located at the ends of the bone specimen. The components intended to take measurements were chosen based on cost, reliability, and precision. The displacement sensor was readily available at no cost and found to be accurate for the needs of the project. The load cell being used was chosen since it was inexpensive and can withstand the 2000 newton force being applied to the bone specimen.

Preliminary Data

Table 4: Load Cell Specifications

Specification	Units	Value
Rated Output	mV/V	0.9468
Non-linearity	%FS	0.099
Hysteresis	%FS	0.099
Repeatability	%FS	0.089
Creep	%FS/30 min	0.178
Zero balance	%FS	±1
Input impedance	Ω	350±5
Output impedance	Ω	350±5
Excitation voltage	VDC	9-12
Safe overload	%FS	120

The image of our load cell specifications shows that this force sensor meets our design needs. Having a non-linearity within 0.099% of full scale (FS) and repeatability within 0.089% of FS shows that this sensor can meet precision requirements. Computing these values shows that force measurements collected by this specific sensor should be taken within two Newtons.

Table 5: LVDT specifications

DC 750/SE 750 General Specifications

Input Power (DC 750)	± 15 V DC, $\pm 5\%$, ± 25 mA (nom.)
Input Power (SE 750)	24 V DC (nominal)
	15-24 V DC, 30 mA (nom.)
Full Scale Output (DC 750)	0 to ± 10 V DC
Full Scale Output (SE 750)	0 to 10 V DC
Output Noise & Ripple (DC 750)	<10 mV rms
Output Noise & Ripple (SE 750)	<5 mV rms
Frequency Response (-3dB)	250 Hz (nominal)
Linearity Error	< $\pm 0.25\%$ of FSO
	(< $\pm 0.10\%$ optional, SE 750)
Repeatability Error	< 0.01% of FSO
Hysteresis Error	< 0.01% of FSO
Operating Temperature	0 °F to +160 °F
	-20 °C to +70°C
Thermal Coefficient of Scale Factor	-0.015%/°F (nominal)
	-0.027%/°C (nominal)
Vibration Tolerance	20 g to 2 kHz
Shock Survival	100 g, 11 ms

It can be seen from this image that the LVDT was able to meet the precision requirements detailed in this project. Linearity error was less than $\pm 0.25\%$ full scale output (FSO) (within 0.065 mm) and repeatability error was less than 0.01% of FSO. This means the LVDT can take accurate displacement readings and reproduce the same results after undergoing multiple tests.

Table 6: Linear actuator specifications

Wiring	Bipolar
Operating voltage	5 VDC
Current/phase	3.12 A
Resistance/phase	1.6 Ω
Inductance/phase	8.8 mH
Power consumption	31.2 W
Rotor inertia	1760 gcm ²
Temperature rise	135°F (75°C) Rise
Weight	5.1 lbs (2.3 Kg)
Insulation resistance	20 M Ω
Max applicable force	2000 N

The Haydon Kerk 87000 Series bipolar linear stepper motor would provide the optimal method of applying compressive forces up to 2000N based on its design specifications. More specifically, the bipolar stepper motor utilizes a negative and positive charge to rotate the threads which move the lead screw. This polarity between two electromagnetic coils, or phases, creates a stronger magnetic field and thus provides more torque when turning the threads. The minimal DC power usage also provides the ability to use minimal power supplies as long as they provide the necessary current per phase (3.12Amps) to generate the electromagnetic polarity.

Chapter 5: Design Validation

To assure that all aspects and components of the device are functioning properly, testing protocol is necessary. A running test will not only determine if the device is working as intended, but it will also display any errors that need to be fixed. This makes testing protocol effective in designing an ideal device that can produce repeatable results in a controlled setting. Each component of the device undergoes specific testing protocols to ensure correct functionality. Individual component testing will not only show that each part is functioning correctly, but will also show that everything will work properly within the device when it is taking an image of a bone sample. Furthermore, testing protocol can determine ease of use and that there is good communication between the user and the device.

Circuit Validation

It is crucial that the circuit which powers the sensors on the device and that outputs data be wired carefully. In order to do so, it is suggested that a black box diagram be drawn, showing how the components are intended to be connected to one another. Afterwards, a more detailed and complex circuit diagram can be made from the black box diagram. This will show the interconnecting components along with any other necessary circuitry items that will aid in the operation of the device. These items include resistor wires, op-amps, voltage dividers, capacitors, etc. Some or all of the mentioned items may be used in the circuit depending on how much voltage is needed for each sensor to work.

1. Design circuit with a black box diagram.
2. Expand the black box diagram by adding in circuitry components.
3. Build circuit.
4. Make sure the input voltage is at the expected level.
5. After building is complete, troubleshoot the voltage at each junction using a multimeter.
6. Plug the multimeter probes into the multimeter, paying close attention to the polarity (red is positive, black is ground).

7. Choose a multimeter function using the dial on the machine. The electrical schematic of the bread board will show whether an AC or DC voltage is present.
8. Insert the probes at each junction, moving along the circuit from left to right.
9. Compare the expected voltages with the measured voltages at each junction.

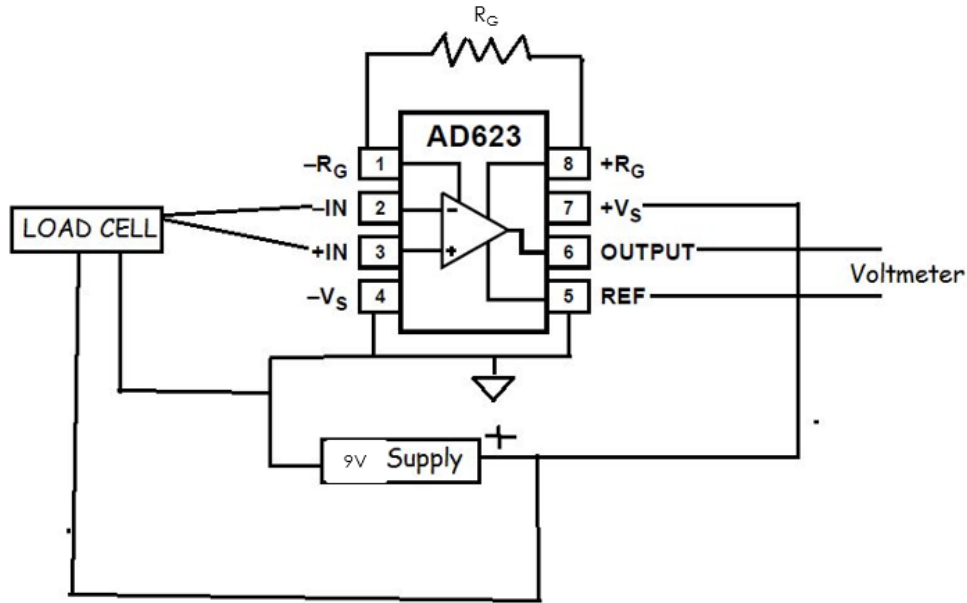


Figure 11: Operational-Amplifier Circuit for Button Load Cell

At the reference pin and ground pins, we expected a voltage of zero, which was observed. The positive and negative grounds have roughly 4.5 volts going in. When comparing just the positive and negative outputs of the load cell, there was a zero to nine mV change depending on the load being applied. Finally, when checking the output voltage to the reference, we found a total gain of 333.

Load Cell

Validation for the load cell begins with calibration and determining the sensor's offset. The offset varies between load cells, making it necessary to measure before the load cell is used for any application. To measure the offset, the load cell should be connected to the circuit and

then placed on a flat surface without applying any force to it. A multimeter is then used to measure the output in mV/V. This output without any force applied is the offset. With the offset determined, a known weight is placed onto the load cell. The measured output from the known weight is recorded and used to determine A, which is the gain value that changes dependent on the desired unit of force or weight to be measured. The values for offset, force, and measured mV/V should now be known, and used to solve for A in the following equation:

$$F = A \cdot (\text{measured mV/V} - \text{offset}) \quad (3)$$

It follows that by solving for A in equation 1 that the gain will be:

$$A = \frac{F}{(\text{measured } \frac{mV}{V} - \text{offset})} \quad (4)$$

Now that the load cell is calibrated, the measured voltage outputs from different loads can be converted to the desired units of force, such as Newtons, pounds, or kilograms.

Further validation can be done once the load cell has been calibrated. Since the force will be distributed within the moving steel plate, the load cell has to be mounted onto this plate before testing protocols can begin. Afterwards, several objects of varying known weights were be carefully placed onto the plate to test the load cell's ability to accurately measure force. The objects used were weights in increments of five pounds, ranging from zero to twenty pounds. Each object was placed on the sensor, and the voltage output was measured using a multimeter. This was done for each increment five times to ensure precision. Afterwards, the average voltage for each increment was calculated and plotted against the known weight. The resultant curve was observed to validate the load cell's linearity and repeatability specifications.

1. Calibrate load cell
 - a. Connect load cell to the circuit.
 - b. Place load cell and circuit on a flat surface.

- c. Using a multimeter, measure and record the voltage output when there is no force on the load cell. This value is the offset.
 - d. Place a known weight onto the load cell.
 - e. Record the voltage output produced by the known weight.
 - f. Determine the necessary gain for the load cell by solving for A in equation 4.
 - g. Apply the gain needed in order for the load cell to take measurements in the desired units of force.
2. Place the steel plate with the attached load cell on a table. The load cell should be facing down.
 3. Collect weights.
 4. Carefully place the weight onto the plate.
 5. Record the force determined by the load cell.
 6. Compare the experimental and calculated values.
 7. Repeat test multiple times to ensure accuracy and precision.

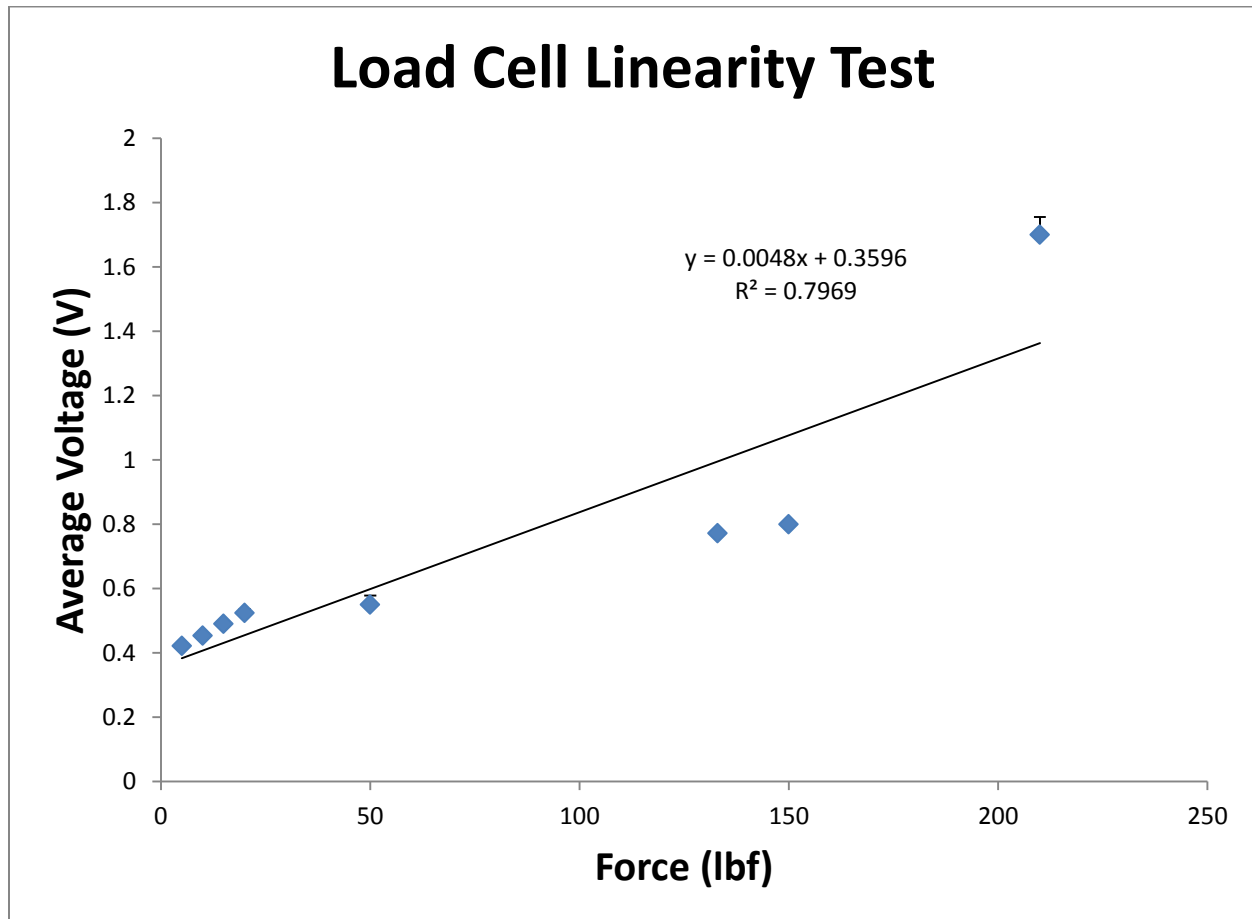


Figure 12: Force to Voltage Comparative Chart

Load cell validation was done in two tests. In the first test, the force sensor was on a hard, sturdy surface. This allowed for stable load distribution, showing a linear relationship between average voltages and increasing load. In the second test, the sensor was on a softer surface prone to unstable loading. The force may not have been perpendicular to the button on the load cell. The button was only 2.5 mm in diameter making it difficult to balance an applied load onto the sensor perfectly. This produced deviations in the voltage output, which can be visualized with the dip in the curve above. Additionally, the softer material dented, causing the load to be applied on the load cell itself, but not on the button.

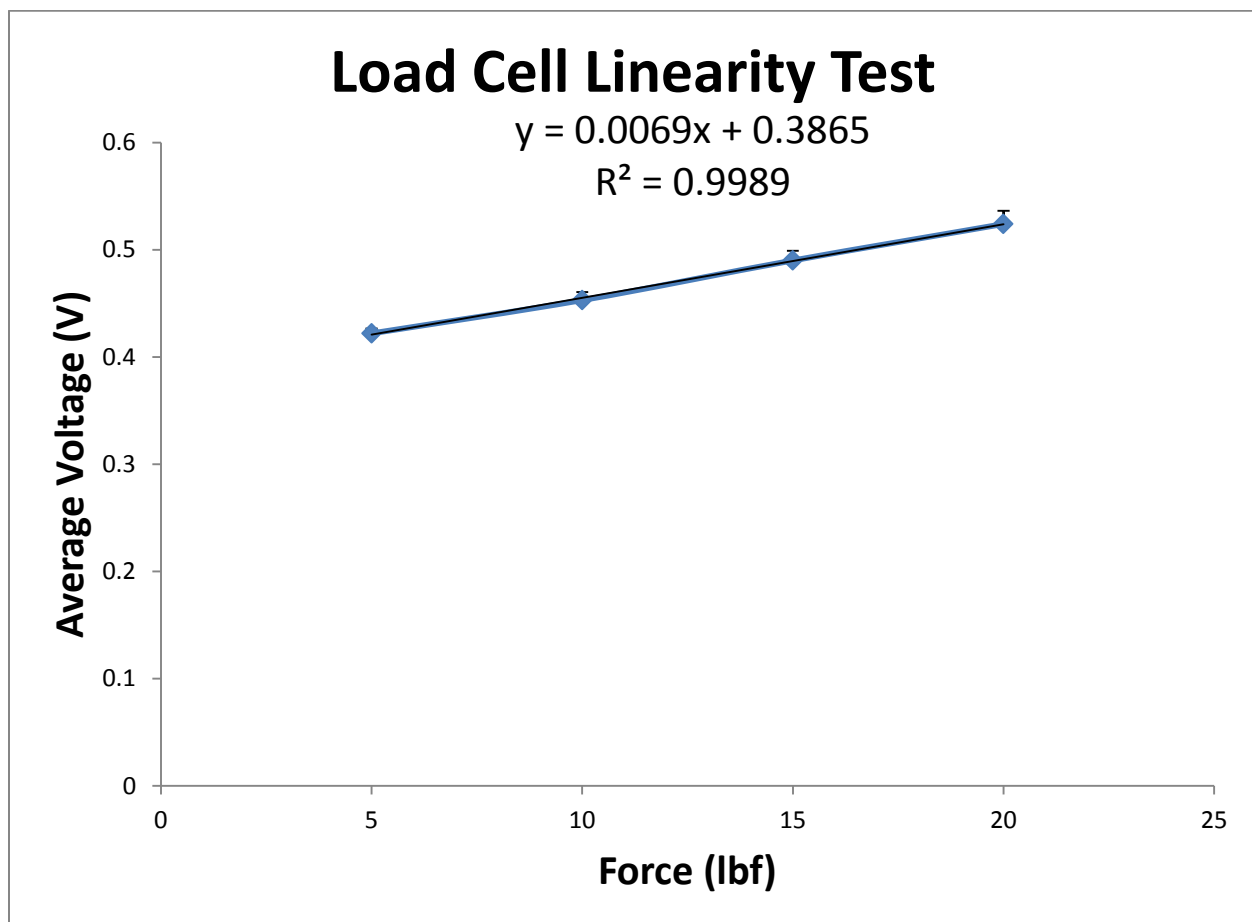


Figure 13: Expected curve if free moving plate does not deform

Figure 13 above shows a plot of the first four data points and the expected loading curve if the applied force does not deform the backing material and is applied almost completely perpendicular to the button.

Stepper Motor

The stepper motor converts mechanical energy into electrical energy via rotation of a motor shaft. To show that the motor is able to generate electrical energy, an LED is connected to the motor. Afterwards, the shaft is rotated manually. If the LED lights up, the test shows that the mechanical energy from rotation of the shaft is indeed being converted to electrical energy.

1. Place motor on table top.
2. Connect LED to wire leads on the motor.
3. Manually rotate the motor shaft and observe if the light turns on.
4. Complete multiple rotations to ensure electrical energy is being generated.

During testing, the stepper motor was able to supply electrical energy to the internal electromagnetic phases, which supply the ability to move the lead screw either forward or backward depending upon the programming of the microcontroller. However, this test lasted for only twenty seconds, as there were troubleshooting issues arising in the circuit connections between the wiring of the electric motor to the microcontroller. Since the tests could not last for a significant amount of time, no meaningful data was obtained.

Displacement Sensor

A caliper is placed alongside the device, parallel to the sensor and movement. The device will then drive the sensor to a certain distance that is measured with the caliper. The displacement value given by the sensor will be compared with the known value to ensure accuracy. Testing will be repeated multiple times to determine the precision of the sensor. The

next step in the testing protocol for the displacement sensor is to examine how well measurements are taken when a sample is in the device. A sample of a known length will be placed in the device and loaded. The displacement of the sample will be measured with a caliper. Afterwards, this value is compared to the displacement value given by the sensor. Again, testing will be repeated multiple times to ensure precision. Lastly, protocol is needed to show that the sensor goes back to zero displacement after the user is finished taking an image. When the sensor is driven back to the origin on the device, it should read that there is zero displacement. If the sensor does not read zero when it is driven back, it will show that there is a calibration issue.

1. Place device on a table top.
2. Place caliper on the table top parallel to the displacement sensor. The caliper should not be touching the device.
3. The caliper should be placed so that the zero position is also where the edge of the moving plate is.
4. Turn on the device and have the sensor move up to a certain displacement that is measured with the caliper.
5. Compare the measured displacement with the value given by the sensor.
6. Return the sensor back to the zero position and ensure that the sensor returns a value of zero displacement when it is at this location.
7. Repeat test multiple times to ensure precision.
8. Place a sample of known length in the device and apply a force to it.
9. Measure the sample's displacement with the caliper.
10. Compare the measured value with the value given by the displacement sensor.
11. Repeat test multiple times to ensure precision



Figure 14: Set up for LVDT validation testing

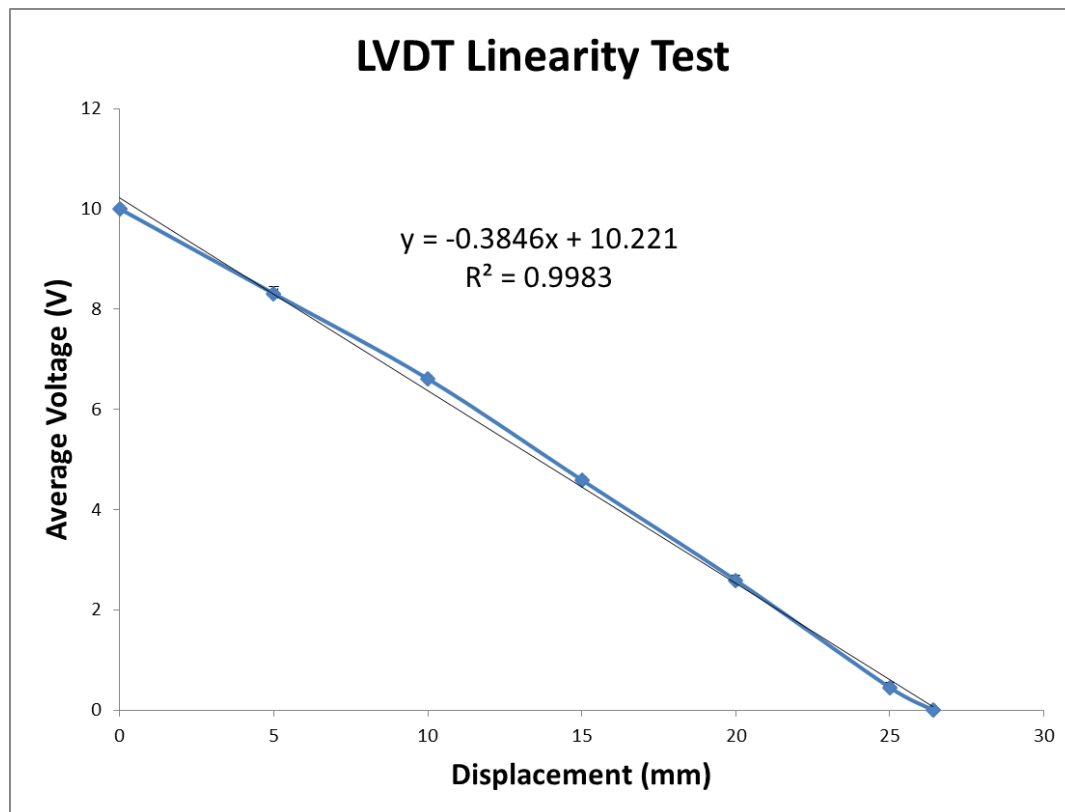


Figure 15: Displacement to Voltage comparative graph

The plot shows a nearly perfect linear relationship between known displacements and average voltages output by the LVDT. This justifies that the LVDT can meet the loading device's precision needs. We can conclude that the LVDT can collect accurate displacement measurements and reproduce these readings if the same test were performed multiple times.

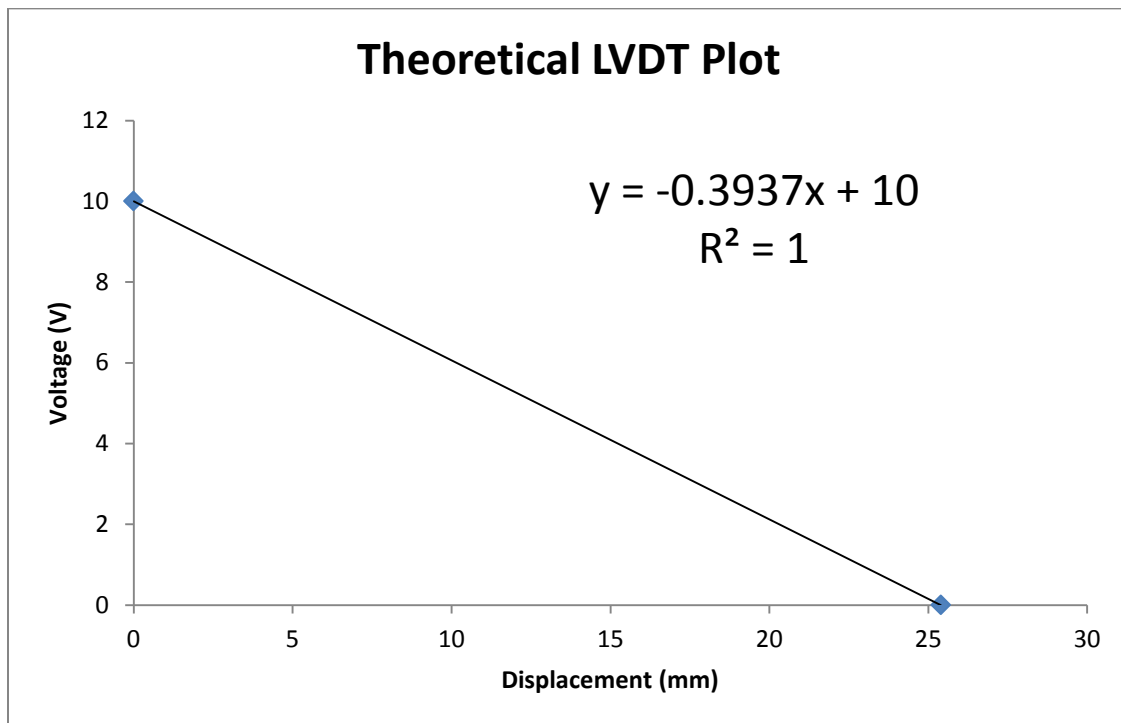


Figure 16: Theoretically determined LVDT plot

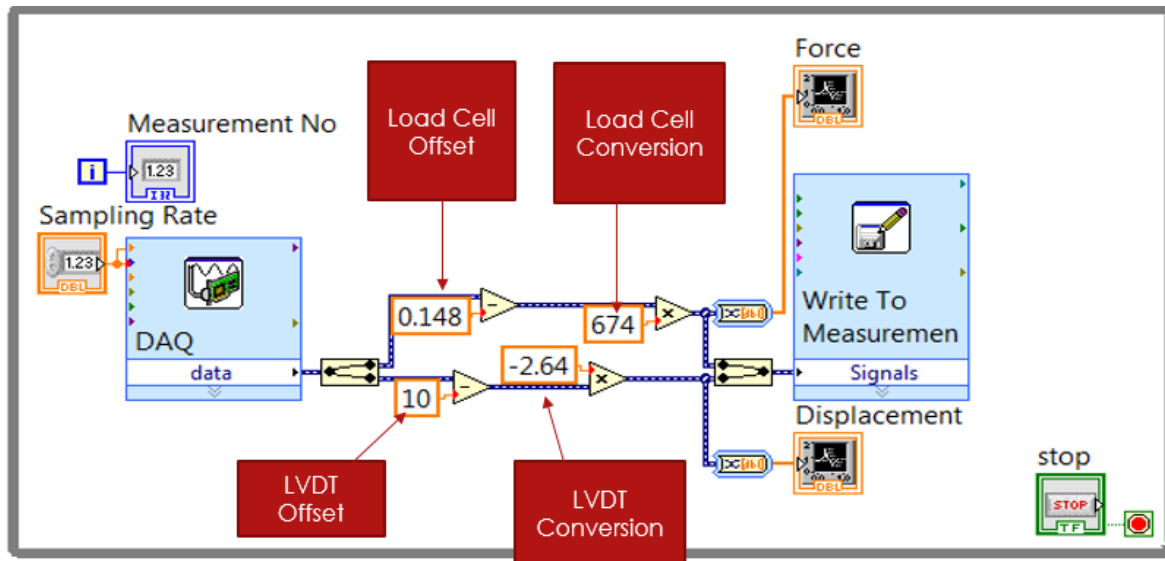


Figure 17: Block diagram of user interface

Data is transmitted to the program through the DAQ assistant, which is represented by the DAQ block on the left. The data is then split into the force and displacement voltages. An initial voltage was measured for both the load cell and the LVDT that need to be subtracted from the signal seen in the offsets. These zeroed signals are then converted into their respective units. The load cell had a maximum output voltage range of 3 V which was used along with its 2000 N max to calculate a 674 V to N conversion factor. Similarly, the LVDT had a max displacement of 26.4 mm and voltage range of 10 V. These were used to calculate the conversion factor. Because the LVDT had a output voltage of 10 V for zero displacement, and a zero voltage for maximum displacement, the maximum signal range had to be changed to -10V instead of +10V. Because of this, the conversion factor had to be -2.64 V to compensate.

Chapter 6: Discussion

Assumptions

Several assumptions were made before the final fabrication of the loading device. The sensors were expected to work when the circuiting was fully assembled, which would conclude that data can be obtained from utilizing the loading device. In addition, the metal plates were assumed to be strong enough to compress many samples of specimens without the risk of deformation. The PVC piping was also assumed to be strong enough to sustain the housing of the loading device and compressive load upon the specimen while also allowing the x-rays to pass easily to accurately image the specimen. The final assumption of the loading device is that the free-moving plate will not lock up with the PVC supports or the lead screw when compressing the specimens.

Precision and Accuracy

To determine the precision of both the force and displacement sensors, a series of five tests were conducted on both sensors to determine the mean and standard deviation of each voltage value at several different loads or displacements. The final results of these tests concluded a relationship in which the standard deviation values for both the force and displacement voltage readings were less than one percent of the mean voltage readings at specific force and displacement values. Thus, it was determined that the sensors are precise.

The accuracy of the sensors can be determined by the linear relationship of the graphs shown in Figure 12 through 16, in which an R^2 value of roughly 0.99 was attained. When we create a theoretical line seen in Figure 16, and compared the experimentally determined linear fit

line, the slope was only off by 0.009. This shows that the LVDT is accurate, while the load cell accuracy is discussed in the limitations section.

Limitations

Stepper Motor

The original fabrication of the radiolucent loading device included an electrical stepper motor as to provide the user with an automated method of compressing bone or other materials without removing the entire device from the CT scanner. However, several issues arose with the setup of the motor and its components both within the programming of the microcontroller and the circuiting. The programming was originally unable to communicate with the motor, so several adjustments were made to both the programming by including more controller pins. In addition, the circuit had to be upgraded from DC to AC power due to the lack of current provided by a 9V battery. A 9V battery would only supply a 200mA current per phase within the electrical motor, which required 3.12A per phase. The upgrade to AC power provided 1Amps per phase for the motor, and was able to move the lead screw forward. Further troubleshooting issues arose after 20 seconds of running the motor, as the circuit connections between the microcontroller and the motor were not producing a complete circuit. Due to time constraints, a hand crank was substituted for the motor in order to attain data for final analysis.

Electronics

Several troubleshooting issues arose when constructing the electronics of the loading device for supplying real-time data of both force and displacement. To begin, the operational amplifier that was being utilized for the load sensor would only give 1/3 of maximum gain it was

intended to provide based off of the AD623 datasheet. More specifically, the op-amp would only provide a 333 gain out of the 1000 gain that it could provide. When the maximum gain was used, the output voltage would max out with only 70 Newtons of force and not change when more force was applied. In addition, the op-amp was tripling the input error between the sensor and the data acquisition (DATAQ) device.

Due to time constraints, the circuiting and electronics could not be completely soldered for the final product. This provided a troubling limitation, as the circuiting would be a lot less stable; thus, the electronics and the loading device housing have to be separated during transportation to limit the risk of damaging the fragile electronics.

To compensate for the necessary 12V of input energy for the force sensor, and the 24V of input energy for the LVDT, the original design of the loading device incorporated a single 24V power supply for both sensors that would be divided in half for the load sensor. A decision was made to separate the power supplied in order to simplify the circuit. The LVDT used a power supply of several battery packs that are connected in series to provide the necessary 24V of input power. The load sensor used a 9V battery pack, which was within the required input voltage necessary to operate the button load cell.

Finally, communication between the sensors and the DATAQ device produced several limitations for the group during assembly. The input error of the DATAQ itself was 5mV, which caused a 5N error for the force reading. While this was within the design specifications, the force sensor also had an inherent sensor error, which combined with the DATAQ input error would produce a total sensor error of 8N. While this force reading error is above our design specifications, it is not significant because when the maximum gain is achieved from the op-amp, the input error should be reduced to a third, putting us within the specifications. In addition, if

the operational amplifier produced its maximum gain, then the total error of the force reading would be within the design parameters.

Testing

During the final round of testing for the load cell, a softer compressive surface was used which at higher compressive loads would deform. This deformation would cause a rapid decrease in the voltage readings of the load cell, which provided mixed results for the final graphical analysis. This phenomena can be seen previously in Figure 16. Although this test provided abnormal data, taking the first four points should not have suffered from the faulty loading surfaces can represent the expected loading curve. To determine this, a theoretical weight value of 210lbs was applied to the linear relationship function found using the first four points and compared to the experimentally determined results. In previous tests, 210lbs was displaying a mean voltage value of 1.78V. When the theoretical value was used, the calculated voltage was 1.83V, which demonstrates that the linear fit and sensor are accurate and reliable.

Impact of Our Device

Economics

It is estimated that the materials used to build the device are cheap enough so that several units can be made for sale while also allowing the manufacturer to make a profit. The majority of the components for the device are relatively low cost. Steel pieces and PVC piping were used to make the compression plates and support rods, respectively. To generate force, a \$10 hand crank utilizing a worm gear was integrated into the device. The large portion of the manufacturing cost will come from the sensors. For the purposes of this project, a \$45 compression button load cell and a \$100 DC-operated LVDT (750 series) position sensor were used to take the different measurements. Overall, total manufacturing costs will be approximately \$400, however this can

change depending on the availability of materials with better mechanical properties and more precise sensors.

Environmental Impact

The risk of the loading device being an environmental concern will be minimal. The product will be mainly used for further research in hospital and laboratory settings. The steel used for the compression and fixed plates can be easily recycled. It is well known that steel is one of the most recycled materials in the world. Steel possesses excellent metallurgic properties that allow for continual recycling while still maintaining its mechanical properties and without hindering performance from device to device. PVC has proven to be a polluting plastic due to the toxic chemicals that are released into the environment as time passes. However, measures can be taken to safely recycle PVC. Mechanical recycling can be done to recycle PVC into a base powder that will be used for a different application. PVC can also be chemically recycled to alter the material at a molecular level. This will effectively remove chemical additives and other harmful products to develop a healthier and more environmentally friendly material.

Societal Influence

One of the main goals of the loading device was to make it radiolucent so that it will be fully operational within the confines of a CT scanner bore. The benefits of having a functional loading device inside of a CT scanner is that images can be collected that show the microstructure of bone samples under varying degrees of compression loading. This information is useful to medical professionals since it can determine the extent of an injury caused by too much compressional loading of a bone.

Politics

The product's effect on the global market is contingent on the success of the device during initial sales once it reaches national distribution. If there is a large enough demand for the product, manufacturers can expand to international distribution. This would allow people in other countries to use a novel piece of technology, and improve upon current work.

Ethics

There will be minimal ethical concern for the project since loading devices do not create controversy in terms of their development and performance. There is also little ethical concern behind the selection of materials for the device since they are recyclable and will not be majorly harm the environment. Minor ethical concerns may arise with the use of cadavers for testing. Most of these concerns are addressed if cadavers are obtained through the proper channels.

Health and Safety

The device is intended to be used with bone samples and not actual human subjects. Furthermore, images will be taken in a controlled setting, such as in medical facilities and laboratories. If proper protocol is followed in the use and handling of biological specimens, there should be minimal health and safety risks associated with our device. Due to these factors, there is no concern for the safety and well-being of others when the loading device is operational.

Manufacturing

While there are no immediate plans to create more units, the device could be easily manufactured by distributors in a factory setting. This is possible given the availability of materials, sensor components, and a working knowledge of electrical and computer engineering.

Sustainability

The device will utilize battery packs to power the different sensors incorporated into the final design. These are not classified as renewable and need to be recycled when they have reached the end of their life cycle. Measures will need to be taken using renewable resources if manufacturers would like to make this product more energy efficient.

Chapter 7: Final Design and Validation

After gaining a better understanding of the problem and establishing a product need, a novel radiolucent loading device for computed tomography imaging was constructed.

The final design consists of three rectangular steel plates, whose cross section is cut to allow easy access into a 7.5" x 5" CT bore. A circular steel disc is mounted in the center of one of the steel plate cutouts intended to be the free moving plate that supports a force sensor and the central core rod of a LVDT. The disc is attached using screws and bolts, leaving enough space in between the disc and plate for the force sensor. The other two steel cutouts are end plates that remain fixed. One will be used to hold the specimen as it is being compressed while the other will support the LVDT and support a lead screw passing through its center that will push on the free moving plate. At each corner of the steel plates is a 27.2 millimeter hole to allow entry for a piece of PVC piping. Four PVC rods of approximately 31 inches in length are used to connect and align the three rectangular plates parallel to one another. Epoxy with a load bearing capacity of (number) PSI is used to secure two steel plates at the ends of the PVC tubes while the third plate that houses the load sensor is left in between the epoxied plates to move freely in a unidimensional motion. Steel was chosen because its strong mechanical and material properties allow for stable and heavy compression. PVC was chosen since it will not obstruct x-rays that are scanning the specimen and will not alter the final CT image.

To measure force, a 3137 compressive button load cell from Robotshop.com with a capacity of 200 kilograms was used. This was chosen as a force sensor since it is small (25x11 mm), low cost (\$45), and met design needs. In terms of design needs, the load cell was precise within 0.2% FS, with repeatability at 0.089% FS and non-linearity at 0.099% FS. The sensor was put on the free moving plate in the area in between the attached steel disc and the steel plate.

This is an ideal placement since the compressive force will act primarily at the midpoint of the half bridge within the load cell. This will allow for a voltage change at this position on the bridge, generating an accurate output that can be measured.

An LVDT was chosen to collect displacement measurements due to its immediate availability in one of the labs on campus and because it met precision standards. Specifically, the LVDT had a linearity error less than $\pm 0.25\%$ of FSO and a repeatability error less than 0.01% of FSO. The central core of the LVDT was positioned through the free moving plate so that it would move as the plate compresses the specimen. The main LVDT tube containing the central core was supported by the fixed plate containing the screw, but was not permanently attached to it. This allows for easy removal of the LVDT and permits the loading device to accommodate for specimens of varying sizes, all without altering the zero displacement value used to calibrate the LVDT.

A threaded rod with a diameter of 0.625 inches and a size 18 thread was utilized as the hand crank. The total length of the threaded rod was 6 inches to allow for the compression of large and small materials in the loading device. To turn the threaded rod either forwards or in reverse, a nut was epoxied to the end of the threaded rod to allow the user to move the rod with a hand wrench. The rod was fixed for movement in one end-plate with a nut, which was welded to the plate.

A LabView virtual instrument was used to create a display of force and displacement readings to the device operator. LabView was chosen since it is easy software to use to collect different types of data at once, and since it integrates DAQ assistants. A DATAQ 6008 from National Instruments was used to communicate the voltage readings from the sensors to the LabView program. The program itself is conditioned to first provide an offset of the voltage

signals, in order to zero any input that may disrupt the accuracy of the force or displacement readings (Fig. 17). The sensor signals were then given a conversion factor, which were both calculated based off of gathered data comparing the voltage to force or displacement measurements. The converted signals would then be shown graphically and tracked in real-time data, which would also be saved as a comma separated file (CSV) in a user designated location (Fig. 17).

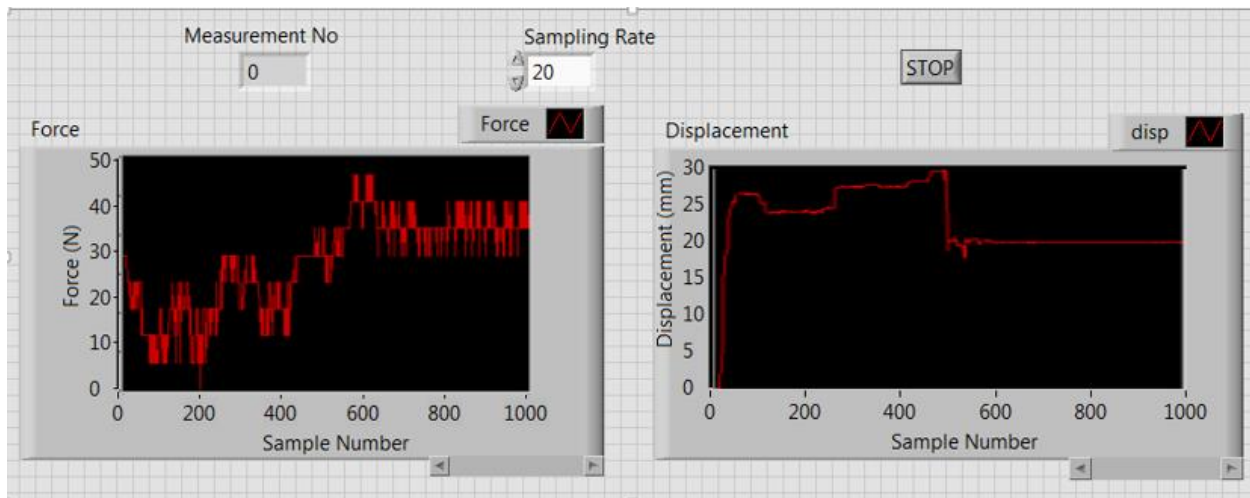


Figure 18: LabView Force and Displacement Graphs

Figure 18 above shows the interface the user will control. There are two graphical indicators, one for force and one for displacement. In the top left there is a measurement number that shows how long the experiment has been running in seconds. The user can control the sampling rate to limit data acquisition during imaging when the force or displacement is being tracked to show consistency. The graphs show the force or displacement on the Y-axis and time in the form of sample number on the X-axis. Sample number was used because when standard time was implemented, it was based off of the internal clock of the DAQ assistant as opposed to the experimental time.

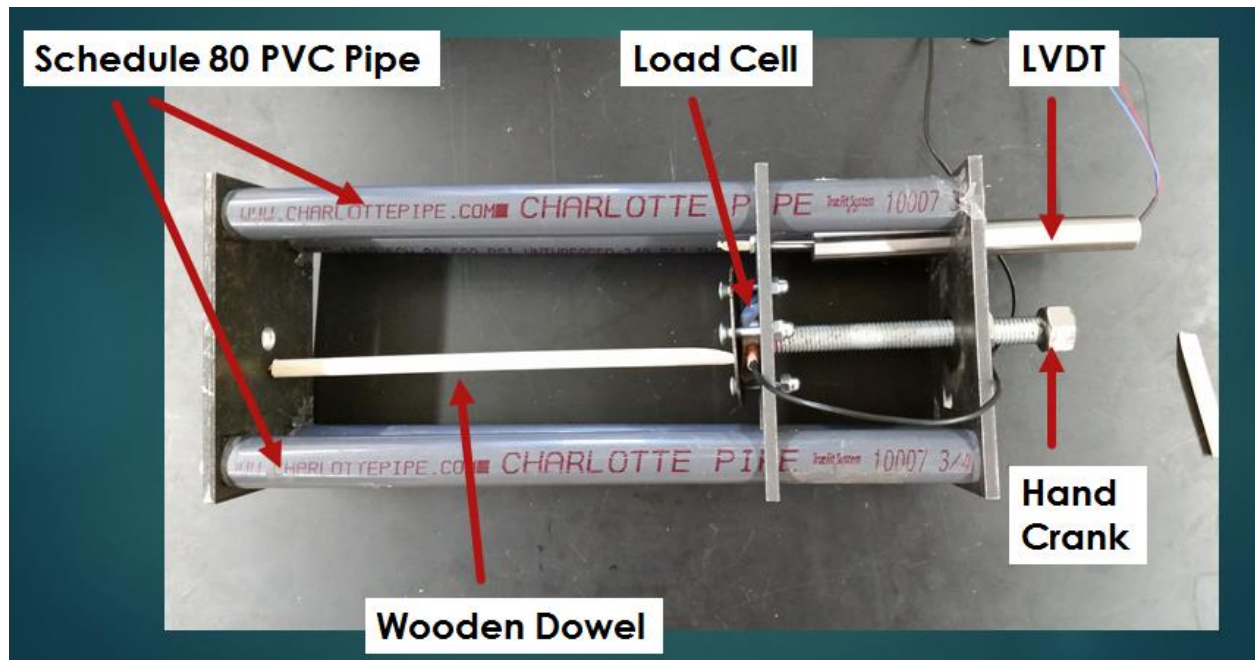


Figure 19: Top view of final prototype

Chapter 8: Conclusions and Recommendations

Conclusions

The goal of this project was to design and fabricate a device that could compress bone or other material specimens within a micro-computed tomography scanner. This device needed to incorporate sensors that would provide both force and displacement data accurate within 5 N and 0.1 mm respectively. The user interface must also be conditioned as to allow for the tracking of real-time data that can be saved to a separate file for further analysis. A final device was fabricated with radiolucent materials, which allowed for the ability to scan dense materials in compression at a microstructure level without interfering with the x-rays for accurate imaging of the materials. Force and displacement sensors were also incorporated within the final fabrication of the loading device; however, the force sensor was accurate within 8 N and thus was not within the design specifications. The displacement sensor was accurate within 0.071 mm and thus was within design specifications. Both sensors were incorporated into the LabView program, which allowed for the tracking of real-time data that could be saved later for the user to further analyze.

Recommendations

Based on the success and shortcomings of the final radiolucent device, there are several recommendations for individuals or groups that can be made in regards towards the fabrication of the second generation radiolucent loading device. To start, the hand crank should be replaced by the electric motor as to provide an automated method of compressing bone or other dense materials. Incorporating the electric motor would require the update of the Arduino Programming to provide the user with full control of the movement of the motor; in addition, the circuiting and wiring between the microcontroller and the stepper motor should be structured so the connections are not loose. Finally, improving the power supply to provide the full 3.12 A

required to drive the motor is necessary. These updates to the electric motor and its components will provide the user with the benefit of having an automated system that will not require the user to remove the loading device each time a new compressive load needs to be applied for each CT scan.

The first generation loading device only provides the ability to compress materials within the CT scanner. However, if the second generation device were conditioned to allow for tensile testing, then the user will have the ability to understand how materials behave in both compressive and tensile stress at a microstructural level. To do this, a third plate should be placed within the moving section of the device. By creating a pulley system between the two outer plates and the inner plate of the moving section, tension can be converted into compression between the specimen plate and the middle plate. Changing the connection between the actuator and the moving plates will allow it to pull the plates as well as push.

The current radiolucent loading device incorporates radiopaque materials to allow x-rays to easily image much denser materials. However, metal was incorporated into the final design of the loading device, and thus the imaging of the bone or material microstructure towards the loading plates will be interrupted by the dense metal plates. If these plates can be replaced by strong radiopaque materials, such as carbon fiber or PVC, then the users will have the ability to image the microstructure of materials where the compressive force is being applied.

The lead screw to free-moving plate connection is also a concern, as the threads on the screw will lock up with the free-moving plate when larger compressive loads are applied. To compensate for this limitation, the future users should condition the threaded rod and the free-moving plate to have a ball-socket connection, which will provide less frictional force and even less with the use of lubricants. This will also allow the plates to be pulled as well as pushed.

Finally, the sensors utilized within the second generation loading device should be conditioned or chosen to fit within the design specifications. While the displacement sensor (LVDT) had a better accuracy than the required design specification, the force sensor (button load cell) had a higher accuracy rate than predicted. By getting a maximum gain from the op-amp we chose, the force sensor would be as accurate as intended and have a much lesser degree of communication error.

References

- [1] Martineau, P. A., et al. "Volar plating of AO C3 distal radius fractures: biomechanical evaluation of locking screw and locking smooth peg configurations." *The Journal of hand surgery* 33.6 (2008): 827-834
- [2] Keyak, J. H., et al. "Validation of an automated method of three-dimensional finite element modelling of bone." *Journal of Biomedical Engineering* 15.6 (1993): 505-509
- [3] De Zee, Mark, et al. "A generic detailed rigid-body lumbar spine model." *Journal of biomechanics* 40.6 (2007): 1219-1227
- [4] Currey, John D. "The effect of porosity and mineral content on the Young's modulus of elasticity of compact bone." *Journal of biomechanics* 21.2 (1988): 131-139
- [5] Weiner, Steve, and H. Daniel Wagner. "The material bone: structure-mechanical function relations." *Annual Review of Materials Science* 28.1 (1998): 271-298
- [6] Rho, Jae Young, Richard B. Ashman, and Charles H. Turner. "Young's modulus of trabecular and cortical bone material: ultrasonic and microtensile measurements." *Journal of biomechanics* 26.2 (1993): 111-119
- [7] Goldstein, Steven A., Ph.D., et al. "Trabecular Bone Remodeling: An Experimental Model." *Journal of Biomechanics* 24.1 (1991): 135-150
- [8] Choi, K., et al. "The elastic moduli of human subchondral, trabecular, and cortical bone tissue and the size-dependency of cortical bone modulus." *Journal of biomechanics* 23.11 (1990): 1103-1113
- [9] Rikli, D., et al. "Assessment and Decision Making." *AO Principles of Fracture Management*.
- [10] Pietruszczak, S., and K. Gdela. "Inelastic analysis of fracture propagation in distal radius." *Journal of Applied Mechanics* 77.1 (2010): 011009
- [11] Solgaard, Seren. "Function after distal radius fracture." *Acta Orthopaedica* 59.1 (1988): 39-42
- [12] Trumble, Thomas E., Susan R. Schmitt, and Nicholas B. Vedder. "Factors affecting functional outcome of displaced intra-articular distal radius fractures." *The Journal of hand surgery* 19.2 (1994): 325-340

- [13] Kwan, K., et al. "Operative Treatment of Distal Radial Fractures with Locking Plate System—a Prospective Study." *International Orthopaedics* 35.3 (2011): 389–394. *PMC*. Web. 27 Apr. 2015.
- [14] Martineau, P. A., et al. "Volar plating of AO C3 distal radius fractures: biomechanical evaluation of locking screw and locking smooth peg configurations." *The Journal of hand surgery* 33.6 (2008): 827-834
- [15] Sobky, Kareem, et al. "Biomechanical comparison of different volar fracture fixation plates for distal radius fractures." *Hand* 3.2 (2008): 96-101
- [16] Cardoso, Luis, et al. "Advances in assessment of bone porosity, permeability and interstitial fluid flow." *Journal of biomechanics* 46.2 (2013): 253-265
- [17] Brenner, David J., and Eric J. Hall. "Computed tomography—an increasing source of radiation exposure." *New England Journal of Medicine* 357.22 (2007): 2277-2284
- [18] "How Does CT Work?" N.p., 2014. Web
- [19] Luan, Hui-Qin, et al. "The application of micro-CT in monitoring bone alterations in tail-suspended rats in vivo." *Advances in Space Research* 53.11 (2014): 1567-1573
- [20] *Mimics Student Edition Course Book*. Ann Arbor: Materialise, 2014
- [21] "FEA Basics." *Biomech.org*. N.p., 2010. Web
- [22] Hambli, Ridha. "Micro-CT finite element model and experimental validation of trabecular bone damage and fracture." *Bone* 56.2 (2013): 363-374
- [23] N. Trabelsi, Z. Yosibash, C. Wutte, P. Augat, and S. Eberle, "Patient-specific finite element analysis of the human femur—A double-blinded biomechanical validation," *Journal of Biomechanics*, vol. 44, no. 9, pp. 1666–1672, Jun. 2011.
- [24] R. Tiossi, M. A. A. Vasco, L. Lin, H. J. Conrad, O. L. Bezzon, R. F. Ribeiro, and A. S. L. Fok, "Validation of finite element models for strain analysis of implant-supported prostheses using digital image correlation," *Dental Materials*, vol. 29, no. 7, pp. 788–796, Jul. 2013.
- [25] S. P. Evans, W. C. H. Parr, P. D. Clausen, A. Jones, and S. Wroe, "Finite element analysis of a micromechanical model of bone and a new 3D approach to validation," *Journal of Biomechanics*, vol. 45, no. 15, pp. 2702–2705, Oct. 2012.
- [26] Haydon Kerk Motor Solutions.
http://www.haydonkerk.com/Portals/0/pdf/Stepper_Motor_Linear_Actuators_101.pdf

- [27] J. J. Wright, "Hydraulic booster device for linear actuator," US5205200 A, 27-Apr-1993.
- [28] H. D. C, "Materials testing machine," US3375709 A, 02-Apr-1968.
- [29] Suzuki, Seiji, et al. "Weighing scale with load cell." U.S. Patent No. 4,196,784. 8 Apr. 1980.
- [30] "Displacement and Position Sensors." - *National Instruments*. N.p., n.d. Web. 28 Apr. 2015. <<http://sine.ni.com/np/app/main/p/ap/daq/lang/en/pg/1/sn/n17:daq,n21:11/fmid/3003/>>.
- [31] http://www.lowes.com/pd_49732-1814-PVC+10010++0400_0__?productId=3356302
- [32] <http://www.analog.com/en/products/amplifiers/instrumentation-amplifiers/ad623.html#product-samplebuy>
- [33] <https://www.sparkfun.com/products/12779>
- [34] https://www.sparkfun.com/products/12859?gclid=Cj0KEQjwgoKqBRDt_Iflr8y1iMUBEiQA8Ua7XaC_EJGrMFNyIid351csJtxc--ylCL1DFp1uPjMGeK4aAhVD8P8HAQ

Appendix

Engineering Drawings

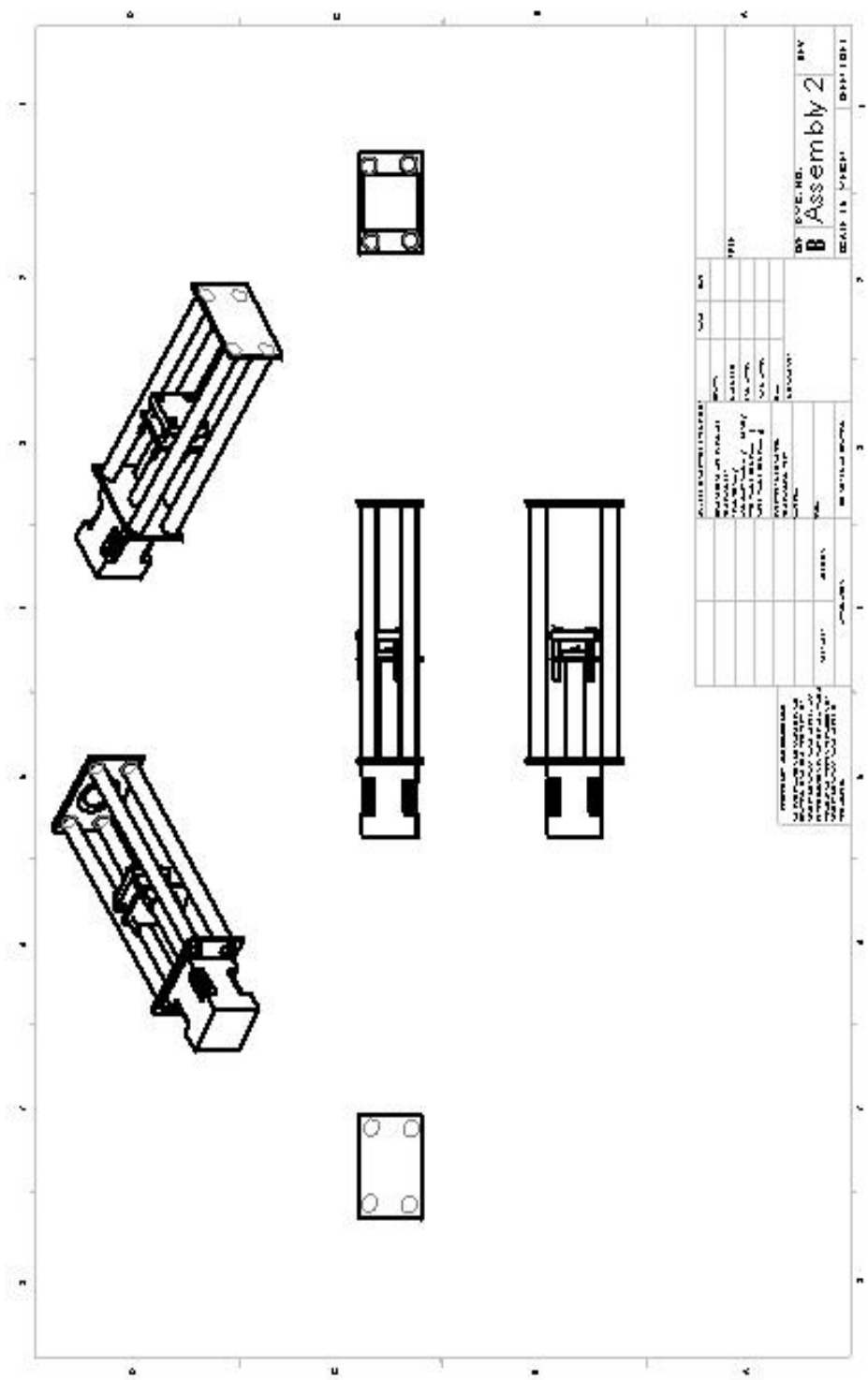


Figure 20: Initial design

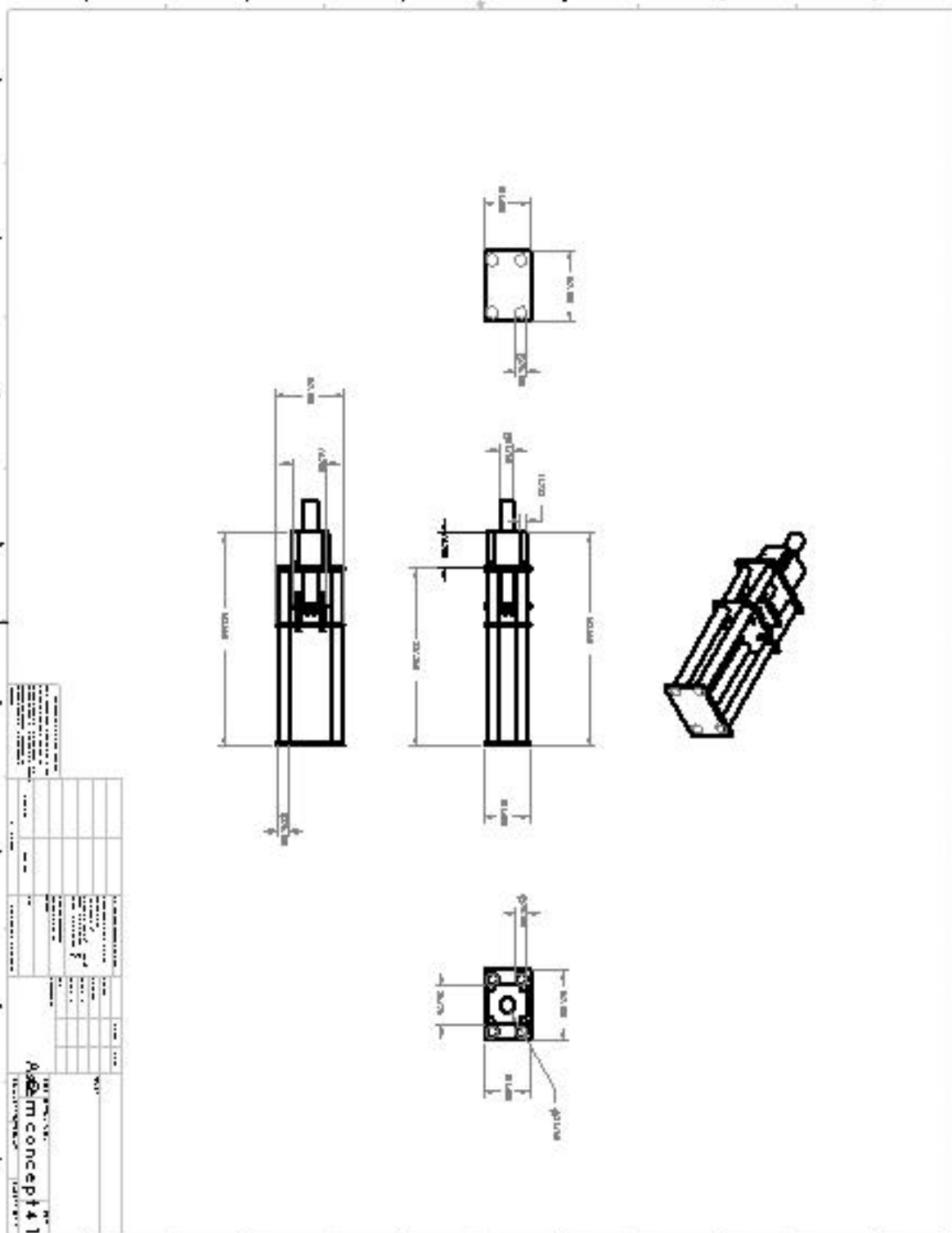


Figure 21: Final design assembly

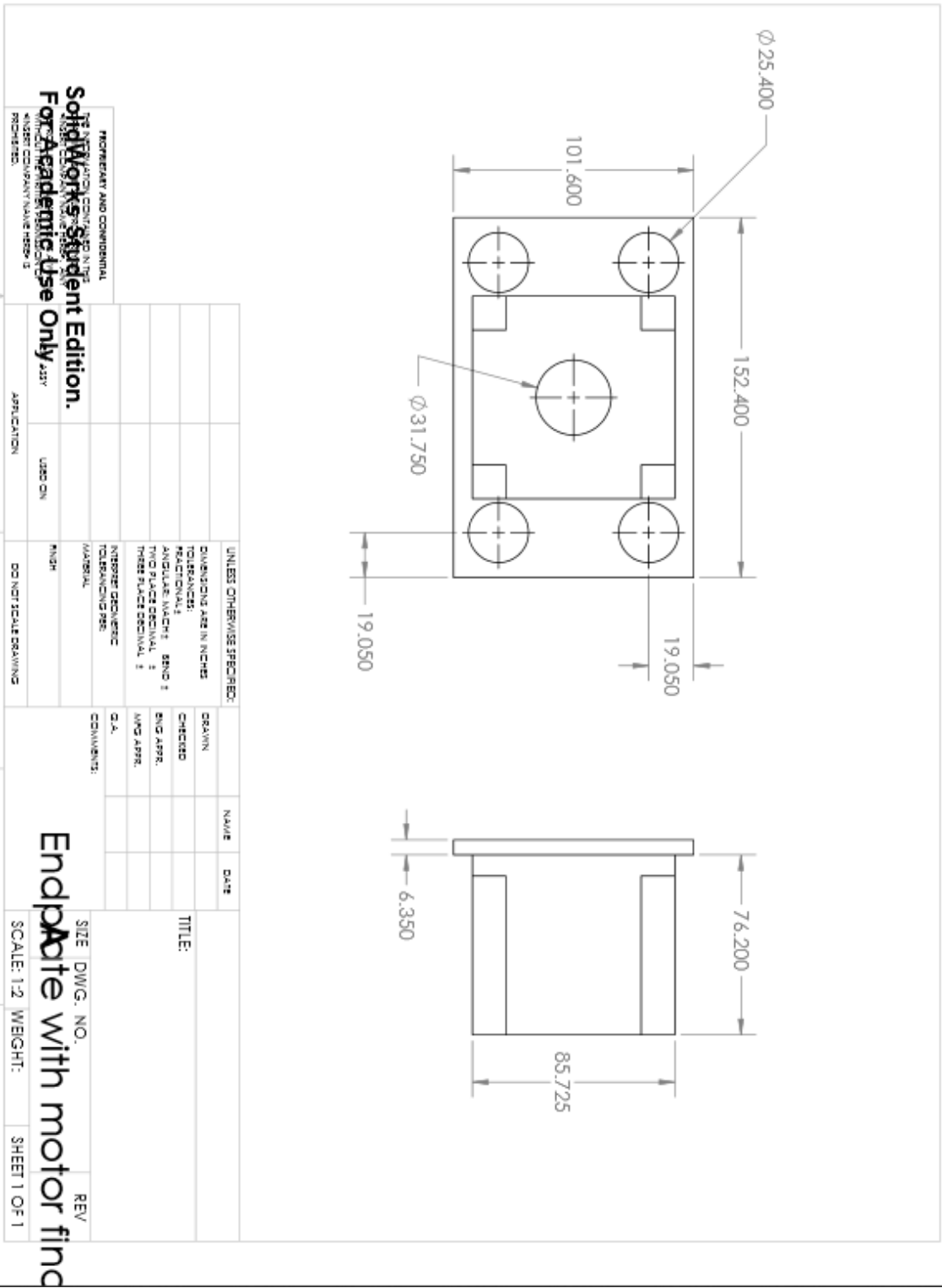


Figure 22: Motor plate cross section

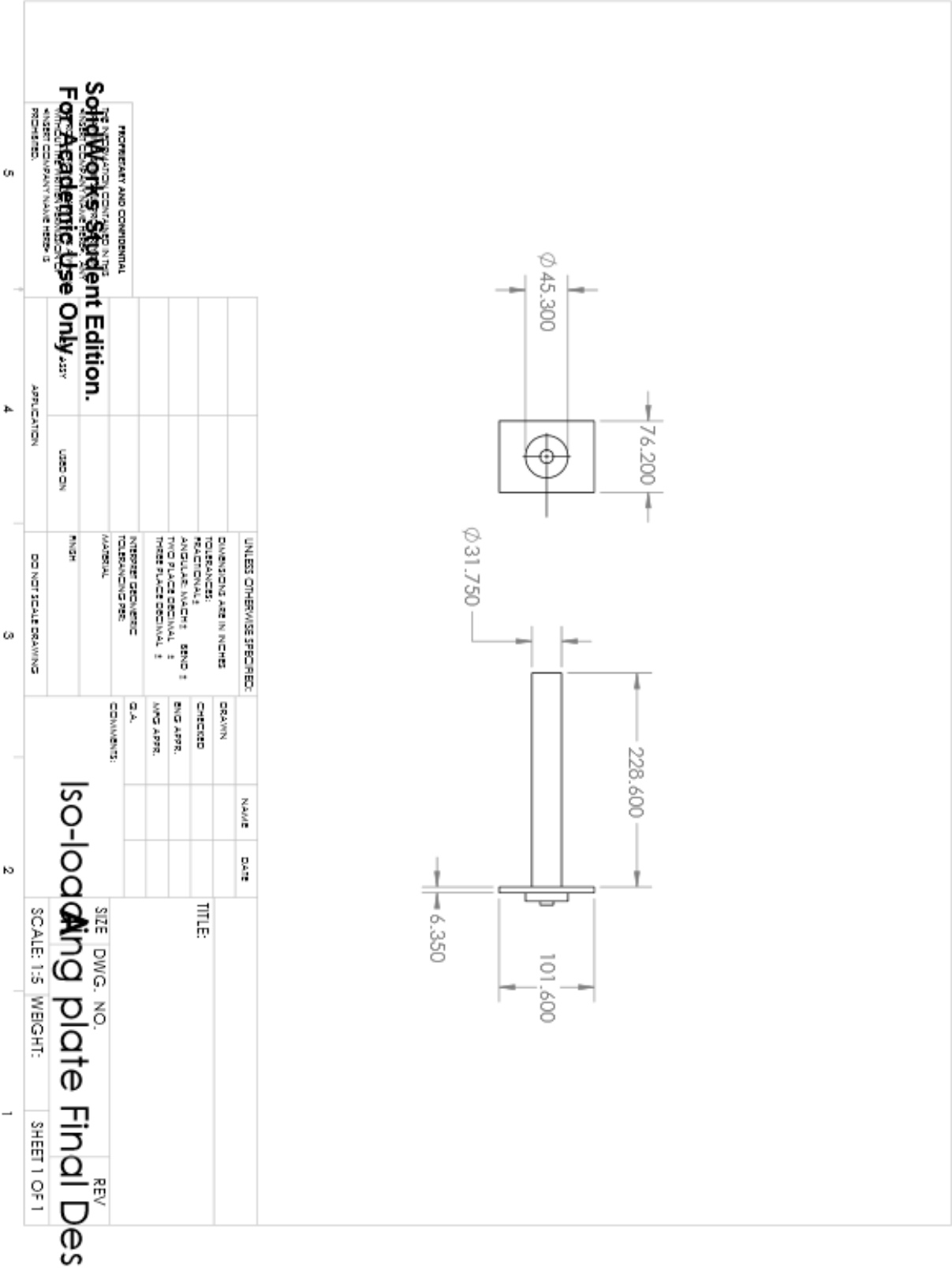


Figure 24: Lead screw assembly

Bill of Materials

Table 7: Bill of Materials

Bill of Materials				
Item	Quantity	Price (\$)	Specs	Sources
Schedule 80 PVC pipe	1	27.98	1in x 20ft 680PSI	[31]
linear stepping motor	1	252	Haydon Kerk 87000 Series Size 34 Linear Stepper M	Quoted from Company
Metal Plates	3	30	2 lrg, 2 small	Price From Lowes
Metal Rods (iso plate)	1	free		Price From Home Depot
Loading Cell	1	45	Button Load Cell	Price on RobotShop
LVDT	1	free	N/A	Provided by Advisor's Lab
AD623 Op-Amp	1	5	N/A	[32]
EZ-Driver Microcontroller	2	35	N/A	[33][34]
Wires	30	free	N/A	Provided by Lisa Wall
Batteries	12	free	9V, 1.5V	Provided by ECE Lab
Epoxy	3	15	JB Weld 4000PSI	Priced From Home Depot
Threaded Rod	1	5	6in x 0.625in (length x diameter) type 18 thread	Priced By Home Depot
TOTAL COST		414.98		

Block Diagram

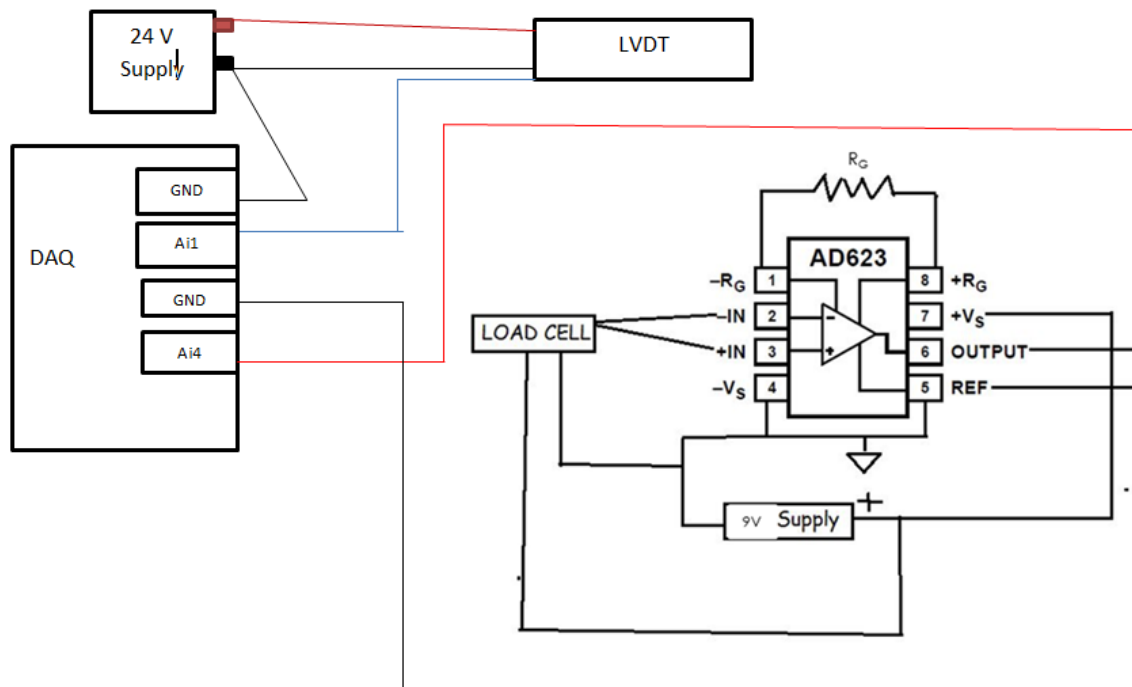


Figure 25: Block diagram of circuitry

Stepper Motor Code

```
int dirPin = 2;

int stepperPin = 3;

int enablePin = 4;


void setup() {

  pinMode(dirPin, OUTPUT);

  pinMode(stepperPin, OUTPUT);

  pinMode(enablePin, OUTPUT);

  digitalWrite(dirPin, HIGH);

  digitalWrite(stepperPin, HIGH);

  digitalWrite(enablePin, HIGH);


  Serial.begin(9600);
}


void loop() {

  if(Serial.begin(9600) = start
  rotate(800, 0.5);

  delay(5000);
```

```

//Serial.println("Hello Galanis\n");

if.Serial.begin(9600) = stop
rotate(0,0);

// put your main code here, to run repeatedly:

}

void rotate(int steps, float speed){
  //rotate a specific number of microsteps (8 microsteps per step) - (negative for reverse
  movement)

  //speed is any number from .01 -> 1 with 1 being fastest - Slower is stronger

  int direction;
  if (steps > 0){
    direction = HIGH;
  } else{
    direction = LOW;
  }

  digitalWrite(dirPin, direction);

  float usDelay = (1/speed) * 70;

  for(int i=0; i < steps; i++){

    digitalWrite(stepperPin, HIGH);

    delayMicroseconds(usDelay);

```

```
digitalWrite(stepperPin, LOW);
```

```
delayMicroseconds(usDelay);
```

```
}
```

```
}
```

```
void rotateDeg(float deg, float speed){
```

```
    //rotate a specific number of degrees (negative for reverse movement)
```

```
    //speed is any number from .01 -> 1 with 1 being fastest - Slower is stronger
```

```
    int dir = (deg > 0)? HIGH:LOW;
```

```
    digitalWrite(dirPin,dir);
```

```
    int steps = abs(deg)*(1/0.225);
```

```
    float usDelay = (1/speed) * 70;
```

```
    for(int i=0; i < steps; i++){
```

```
        digitalWrite(stepperPin, HIGH);
```

```
        delayMicroseconds(usDelay);
```

```
        digitalWrite(stepperPin, LOW);
```

```
        delayMicroseconds(usDelay);
```

```
    }
```

```
}
```